# Recent Progress of All‐Bromide Inorganic Perovskite Solar Cells

# Recent progress of all bromide inorganic perovskite solar cells

*Guoqing Tong*[+]*, Luis K. Ono*[+]*, and Yabing Qi*[*]

Dr. G. Tong, Dr. L. K. Ono, Prof. Dr. Y. B. Qi
Energy Materials and Surface Sciences Unit (EMSSU)
Okinawa Institute of Science and Technology Graduate University (OIST)
1919-1 Tancha, Onna-son, Okinawa 904-0495 (Japan)
*Corresponding author: Yabing Qi, E-Mail: Yabing.Qi@OIST.jp

[+]These authors contributed equally to this work.

**Keywords:** inorganic perovskite solar cells, $CsPbBr_3$, stability, vapor deposition, solution

**Abstract:** Inorganic perovskite solar cells (PSCs) have attracted enormous attention during the past five years. Many advanced strategies and techniques were developed for fabricating inorganic PSCs with improved efficiency and stability to realize commercial applications. $CsPbBr_3$ is one of the representative materials of inorganic perovskites and has demonstrated excellent stability against thermal and high humidity environmental conditions. The power conversion efficiency (PCE) of $CsPbBr_3$-based devices increased significantly from 5.95% in 2015 to 10.91% and storage stability under moisture (~80% relative humidity) and heat (~80 ºC) is more than 2000 h. The outstanding performance of $CsPbBr_3$ PSCs show a great potential in light conversion applications. In this review, we summarize and discuss recent developments of $CsPbBr_3$ based PSCs including the physico-chemical as well as optoelectronic properties, processing techniques for fabricating $CsPbBr_3$ films, derivative phase structures, efficiency, and stability of devices. Finally, the challenges and outlook of $CsPbBr_3$ PSCs in the future are discussed at the end of the review.

## 1. Introduction

Currently, the unprecedented development of organic-inorganic hybrid perovskite solar cells (OIH-PSCs) has drawn much attention because of high efficiency, low-cost processing techniques, and abundant availability of raw materials.[1-5] The power conversion efficiency (PCE) of OIH-PSCs, in the past decade, increased rapidly from 3.8% as reported in 2009 to a certified record of 25.2% in 2019.[6, 7] At the same time, researchers demonstrated large scale hybrid PSCs with certified PCEs of 17.25% and 11.7% for mini-modules (17.277 $cm^2$) and submodules (703 $cm^2$), respectively, under stabilized output conditions.[8, 9] However, phase instability of OIH-PSCs under moisture and heating condition impedes their further application because of the volatility of the organic constituents in these materials (such as $MA^+$, $FA^+$ or mixed cations) and the weak bonding energies between metal cations ($Pb^{2+}$) and halide anions ($I^-$, $Br^-$or $Cl^-$).[10-15] Despite a number of strategies that have been developed to improve the stability of OIH-PSCs (e.g., employment of inorganic cation doping,[16-19] surface modification with stable materials[20-22], advanced encapsulation techniques[23-25]), the intrinsically unstable nature of hybrid perovskite materials is still a pending issue for commercial applications with long-term stability.

Different from OIH-PSCs, inorganic PSCs demonstrate excellent moisture and thermal stability by substituting the organic cations ($MA^+$/$FA^+$) with inorganic ones($Cs^+$).[26, 27] There are three basic types, based on different halides, i.e., $CsPbI_3$, $CsPbBr_3$ and $CsPbCl_3$.[28-31] Detailed discussions about perovskite formation can be found in several review papers focusing on this topic.[26, 32] $CsPbI_3$, as a representative

of inorganic PSCs, has a suitable bandgap of ~1.73 eV.[33] Despite the fact that the PCE of $CsPbI_3$ PSCs is already as high as 19%, the undesirable phase transition from the black cubic phase to the yellow non-perovskite phase at room temperature makes the material unstable.[29, 34] For $CsPbCl_3$, the optical bandgap is above ~3.0 eV, which makes it unsuitable for solar cell applications. Alternatively, $CsPbBr_3$ perovskite has also a larger bandgap of 2.3 eV compared to $CsPbI_3$, but shows a much better phase stability in ambient, which ensures appropriate light harvesting characteristics with long term stability when incorporating $CsPbBr_3$ into a solar cell device structure.

In this article, we review recent developments of $CsPbBr_3$ PSCs. We first introduce the basic properties of $CsPbBr_3$ including the crystal structure, chemical-physical and optoelectronic properties. Then, we discuss the reported fabrication techniques to prepare $CsPbBr_3$ films highlighting the morphologies differences of as-prepared films based on the solution- and vapor-based deposition techniques. Furthermore, we summarize the devices structures and corresponding efficiencies (in Table 1) and the recent developments of $CsPbBr_3$-based PSCs. Finally, we discuss the storage stability under moisture (~20% to 80% relative humidity) and elevated temperatures (50 $^oC$~100 $^oC$) as well as operational stability to provide further insights into the advantages of $CsPbBr_3$PSCs and outline a few promising future research directions.

## 2. $CsPbBr_3$ Properties

### 2.1 Crystal structure of $CsPbBr_3$

In the general crystal structure of $CsPbBr_3$, $Pb^{2+}$ and $Br^-$ ions form a 3D framework

of corner-sharing $[PbBr_6]^{4-}$ octahedra with $Cs^+$ ions incorporated between the octahedral spaces.[26, 35] On the basis of single crystal X-ray diffraction (XRD) data, $CsPbBr_3$crystallizes in the orthorhombic (Pnma) space group at room temperature and transforms to the tetragonal (P4/mbm) and cubic (Pm-3m) phases at 88 °C and 130 °C, respectively.[36] The geometric stability of $CsPbBr_3$ structure can be determined by Goldschmidt tolerance factor (t) as follows:

$$t = \frac{R_{Cs}+R_{Pb}}{\sqrt{2}(R_{Cs}+R_{Br})} \quad (1)$$

where R is the ionic radius. In general, to maintain the high-symmetry of the perovskite structure, it is desirable to have a tolerance factor value between 0.81 and 1.02. Although the $Cs^+$ ion has a smaller ionic radius (1.81 Å) than that of $MA^+$ (2.70 Å) or $FA^+$ (2.79 Å),[17] $Cs^+$ still satisfies the requirement of the tolerance factor in the $CsPbBr_3$ inorganic perovskite ($t$=0.82).[37] In contrast, the radius of other cations i.e., ethylammonium (EA) $[(C_2H_5)NH_3]^+$, guanidinium (GA) $[C(NH_2)_3]^+$, and imidazolium (IA) $[C_3N_2H_5]^+$ are 2.74 Å, 2.78 Å and 2,58 Å, which are larger than that of $Cs^+$.[38] We note that the tolerance factor of $EA^+$(1.06), $GA^+$(1.06) and $IA^+$ (1.02) exceeding 1, which indicates phase instability.

In addition to the $CsPbBr_3$ phase, there are two other derivative phases, i.e., $CsPb_2Br_5$ and $Cs_4PbBr_6$ structures (Figure 1c). The tetragonal $CsPb_2Br_5$ shows a two-dimensional (2D) layer structure. In this derivative phase, Cs ions are sandwiched between two layers of Pb-Br-coordinated polyhedrons. The formation of the $CsPb_2Br_5$

phase is induced by the excessive $PbBr_2$ in the structure and can be understood as follows:[42]

$$CsBr+2PbBr_2 \rightarrow CsPb_2Br_5 \quad (2)$$

$$CsPbBr_3+PbBr_2 \rightarrow CsPb_2Br_5 \quad (3)$$

The reverse direction in Reactions (2) and (3) can take place if the tetragonal $CsPb_2Br_5$ phase is annealed at a high temperature (e.g., 300 °C), and $CsPb_2Br_5$ eventually fully disappears above 400 °C by the following mechanism:[43] $CsPb_2Br_5 \rightarrow CsPbBr_3+PbBr_2$. Besides, $Cs_4PbBr_6$ exhibits a zero-dimensional (0D) structure based on the $[PbBr_6]^{4-}$ octahedra, and the octahedra are separated from each other by CsBr bridges. Similar to the $CsPb_2Br_5$, the influence of excessive CsBr leading to the formation of $Cs_4PbBr_6$ can be explained by the following reactions:

$$4CsBr+PbBr_2 \rightarrow Cs_4PbBr_6 \quad (4)$$

$$3CsBr+ CsPbBr_3 \rightarrow Cs_4PbBr_6 \quad (5)$$

**2.2 Properties of $CsPbBr_3$**

$CsPbBr_3$ films display a yellow color after annealing, which indicates that only light in the short wavelength range can be absorbed. The absorption spectrum edge of the $CsPbBr_3$ film is shorter than 540 nm and the exciton induced absorption peak is located at ~ 520 nm. Tauc plot analyses suggest that the $CsPbBr_3$ thin films possess a large optical bandgap of ~2.3 eV. However, by controlling the ratio of CsBr and $PbBr_2$, the bandgap will further increase significantly from 2.3 eV to 4.0 eV because of the phase transition from the cubic perovskite structure to the derivative phases ($Cs_4PbBr_6$ and $CsPb_2Br_5$). As a countermeasure, substituting the bromide with iodine or replacing lead

dication with tin dication can realize a narrower optical bandgap. However, these strategies usually result in inorganic perovskite films with inferior stability.

Except for the optical bandgap, high carrier mobility and long diffusion length are also important parameters for solar cells. Stoumpos et al. found that the high electron mobility of $CsPbBr_3$ (in the form of single crystals) is up to 1000 $cm^2\ V^{-1}\ s^{-1}$ and the electron lifetime is 2.5 μs.[36] Recently, Zhu and co-workers demonstrated the carrier mobility of 38 ± 11 $cm^2\ V^{-1}\ s^{-1}$ for $CsPbBr_3$ single-crystal microplates.[44] The mobility lifetime product of $CsPbBr_3$ single crystals was investigated by Dirin and co-workers.[45] $CsPbBr_3$ shows a smaller mobility lifetime product (~$2\times10^{-4}$ $cm^2\ V^{-1}$) than that for hybrid perovskites, which was attributed to shorter carrier lifetime. Charge carrier lifetimes of 2-7 μs were previously reported for $CsPbBr_3$ single crystals.[26] The carrier diffusion length of 80 nm was reported for $CsPbBr_3$ films.[46] For $CsPbBr_3$ single crystals, the electrons and hole diffusion lengths were reported to be ~10 and ~12 μm, respectively.[47] Lead halide perovskite systems ($APbBr_3$, A=MA/FA/Cs) favor hole diffusion over electron diffusion, which is demonstrated by Elbaz et al.[48] They found that the diffusion length of holes (~10-50 μm) is on average an order of magnitude larger than that of electrons (1 ~ 5 μm). These high carrier mobilities and diffusion lengths ensure fast charge injection and transport in devices, which is essential for achieving a high photocurrent density.

## 3. Fabrication methods for preparation of $CsPbBr_3$ films

The full coverage and high crystallinity of perovskite films are required to achieve a

high performance in solar cells. Generally, similar to the hybrid organic-inorganic perovskite materials, $CsPbBr_3$ films are usually prepared by the solution-processing technique, for example, spin-coating and dipping. Meanwhile, vapor deposition, including co-evaporation and sequential deposition, is another effective strategy to prepare high quality $CsPbBr_3$ films because the solubility limitation of precursor materials in solvents is not a concern in vapor deposition. Additionally, the vapor assisted solution method, combining the spin-coating processing and vapor treatment, is also utilized to produce high quality $CsPbBr_3$ films.

### 3.1 Solution methods for preparation of $CsPbBr_3$ films

#### *3.1.1 One-step solution method*

Solution processing techniques are a simple strategy based on dissolving the precursor materials into a solvent with a fixed ratio. Usually, for OIH-PSCs, dimethyl formamide (DMF), dimethyl sulfoxide (DMSO), γ-butyrolactone (GBL) and a combination of mixed solvents are used to dissolve the $PbX_2$ and MAI/FAI. However, CsBr is less soluble than $PbBr_2$ in the abovementioned aprotic solvents. The maximized concentrations of CsBr in methanol and DMSO are only 0.07 M and 0.25 M, respectively.[31, 40, 49] The poor solubility of CsBr makes it difficult to prepare the $CsPbBr_3$ precursor solution with a molar ratio of 1:1. The side products, for example, CsBr-rich or $PbBr_2$-rich phase has a significant influence on the morphology and quality of as-prepared $CsPbBr_3$ films. Therefore, it is still challenging to fabricate $CsPbBr_3$ films by the one-step solution method.[50] For example, You et al. reported a one-step spin-coating method to fabricate the $CsPbBr_3$ films by dissolving the CsBr and

$PbBr_2$ into the mixed DMF and DMSO solvent (Figure 2a).[51] The maximum concentration of $CsPbBr_3$ precursor solution is only 0.4 M and it was shown that it is difficult to form a thick and full-coverage $CsPbBr_3$ films by the one-step spin-coating method.

*3.1.2 Two-step solution method*

To overcome the insolubility issue of CsBr encountered in the one-step solution coating method, the two-step solution coating method has been developed for $CsPbBr_3$-based PSCs. 1 M of $PbBr_2$ was first dissolved in N, N-dimethylformamide (DMF) and spin-coated on substrates. After the subsequent annealing at an optimized temperature (80 °C) for 30 minutes, the samples were dipped in a CsBr/methanol solution for several minutes, (Figure2b).[39, 52] The key parameters in the two-step solution method are the precursor concentration, temperature of methanol solution and dipping time.[26] The as-prepared $CsPbBr_3$ films were rinsed with isopropanol and annealed at 250 °C for 5-10 min. This strategy has been widely used in $CsPbBr_3$-based PSCs to form thick, full-coverage, and uniform $CsPbBr_3$ films. In addition, Tang and co-workers proposed a multi-step solution method by spin-coating the $PbBr_2$ and CsBr solution sequentially.[40] As seen in Figure 2c, the CsBr solution was spin-coated six times to optimize material composition. Each of the CsBr spin-coating step leads to step-wise phase transition between the derivative phases ($CsPb_2Br_5$/$Cs_4PbBr_6$) and $CsPbBr_3$ phase. The ideal coverage and grain size can be obtained after four cycles. Liu et al. also developed the same strategy to deposit the $CsPbBr_3$ films.[53] They found that the as-prepared $CsPbBr_3$ films had homogeneous, uniform and highly crystalline grains. The average grain size

was up to 1 μm after annealing. Furthermore, the root-mean-square (RMS) roughness of $CsPbBr_3$ films is below 50 nm.

### 3.2 Vapor deposition methods for preparation of $CsPbBr_3$ films

Solubility limitation of precursor materials in solvents is still a bottleneck to fabricate high quality $CsPbBr_3$ perovskite films. Despite Pal et al. reported an all-solid-state mechanochemical grinding method to synthesize $CsPbBr_3$ powder, which can effectively avoid the solubility limitation of precursor materials and $CsPbBr_3$, the purity of final products is still not satisfy the requirement of solar cells.[54] Therefore, there is an increased interest in vapor deposition strategy. The melting/boiling points of CsBr (~630 °C/1300 °C) and $PbBr_2$ (~370 °C/892 °C) powders are still feasible temperatures in standard physical vapor deposition (PVD) techniques. In addition, the thickness of inorganic perovskite films or precursor layers can be precisely controlled by the quartz crystal monitor (QCM) in order to satisfy the ratio of each component.[55, 56] Furthermore, the vapor deposition strategy can realize the application in large scale devices with good uniformity and high reproducibility. Therefore, vapor deposition is a promising and effective strategy to fabricate high-quality perovskite films with full coverage and good uniformity.[57]

#### *3.2.1 Sequential vapor deposition*

Tong et al. reported a sequential vapor deposition method to produce uniform inorganic perovskite films with controllable chemical composition (Figure 3a).[41] They first deposited CsBr on a substrate with an optimized evaporation rate and then coated it with a $PbBr_2$ film on top. By controlling the thickness ratio of the two precursor

materials, they obtained pure $CsPbBr_3$ and mixed phases ($CsPbBr_3$-$CsPb_2Br_5$ and $CsPbBr_3$-$Cs_4PbBr_6$) as follows:[41, 58, 59]

$$CsBr+PbBr_2 \rightarrow CsPbBr_3 \quad (6)$$

$$CsBr+2PbBr_2 \rightarrow CsPb_2Br_5 \quad (7)$$

$$4CsBr+PbBr_2 \rightarrow Cs_4PbBr_6 \quad (8)$$

The as-prepared $CsPbBr_3$ films display large crystalline grains after annealing in air. The largest size of perovskite grains is up to 1 μm, which ensures efficient carrier transport properties in addition to enhanced light absorption. Additionally, a similar strategy is also developed by Li and co-workers, who prepared $CsPbBr_3$ films by controlling the thickness ratio of CsBr and $PbBr_2$ films to achieve high quality $CsPbBr_3$ films.[60] The films deposited by this strategy showed an ultra-smooth surface with a RMS of 17.3 nm, which is much lower than that made by solution methods. The small RMS leads to a better interface contact with HTL. This strategy is usually performed in high vacuum systems with a typical pressure of $10^{-3}$ Pa that has the added advantage of minimizing extrinsic impurities.

*3.2.2 Co-evaporation deposition*

The co-evaporation method was also developed to fabricate $CsPbB_3$ thin films by heating CsBr and $PbBr_2$ simultaneously.[61, 63] Chen and co-workers investigated the effect of the evaporation rates on the formation of $CsPbBr_3$ thin films at the rates of 5, 15, 25 Å $s^{-1}$ (Figure 3b). They found that the evaporation rate showed a significant influence on the crystallinity and crystal orientation.[61] For example, the lower rate was usually favorable for high crystallinity and (100) and (200) crystal orientation. In

contrast, an inhomogeneous thin film with smaller grain sizes was found when the evaporation rate was too high. Recently, Lei et al. also developed the co-evaporation technique to investigate the formation of $CsPbB_3$ films by investigating the effects of the substrate temperature and evaporation rate ratio of precursor materials.[63] They found that the $CsPbBr_3$ films showed a high crystallinity when the substrate temperature was 300 °C and the evaporation rate ratio of CsBr and $PbBr_2$ was 0.7:1. In addition, a higher annealing temperature could significantly increase the grain size and reduce the roughness of the as-prepared films from 60 nm to 43.7 nm. However, many voids appeared as the treatment temperature was above 550 °C.

*3.2.3 Vapor-assisted solution process*

To lower the cost associated with the high vacuum system, Luo et al. developed a vapor-assisted CVD process (Figure 3c), to realize the fast anion-exchange from $CsPbI_3$ to $CsPbBr_3$ by placing the sample into $Br_2$ environment in a vacuum chamber.[62] In this case, the $CsPbI_3$ precursor films were first deposited by spin-coating onto desired substrates, and then transferred into a quartz tube furnace and heated to 150 °C. $Br_2$ vapor was generated from a commercially available bromine water solution and injected into the hot quartz tube. After several minutes of reaction, $CsPbI_3$ transformed to $CsPbBr_3$ (from light green-yellow to bright yellow color) as follows: $CsPbI_3+Br_2$ (g)→$CsPbBr_3+I_2$ (g). Different from the $CsPbI_3$ films that showed a thick but porous layer characterized by the existence of several random cracks within the film, the $CsPbBr_3$ films presented a dense and compact thin layer with a smooth surface because of crystal lattice compression and the flaws in the $CsPbI_3$ precursor films were healed

by the smaller $Br^-$ ions.

## 4. $CsPbBr_3$ solar cells.

The efficiency of hybrid organic-inorganic PSCs is now up to 25.2% and the highest reported PCE of $CsPbI_3$ PSCs is over 18%.[7, 29] However, the record PCE of $CsPbBr_3$ is still substantially lower (10.91%) because of its large bandgap of 2.3 eV and energy mismatch in the HTL-free structure.[64] To alleviate these issues, some strategies are developed such as A-site [65, 66] or B sites doping,[67, 68] ETL/HTL modification[69, 70] and phase transition controlling[40, 64] to improve the perovskite quality, reduce the energy alignment mismatch in order to achieve high performance. Therefore, there is still room to further improve the performance of $CsPbBr_3$ solar cells. It is worth noting that $CsPbBr_3$ films are much more stable than hybrid organic-inorganic perovskite films and pure $CsPbI_3$ films in terms of thermal/moisture stability and phase stability. Recently, research efforts focused on the HTL-free structure (FTO/ETL/$CsPbBr_3$/carbon) in $CsPbBr_3$ PSCs instead of the conventional configuration (FTO/ETL/$CsPbBr_3$/HTL/Au) in order to realize high stability against moisture and thermally induced degradation. Furthermore, $CsPbBr_3$ can also act as an interlayer to provide a better energy alignment and to passivate detrimental defects in the hybrid PSCs.[71-73]

### 4.1 Electron transport layer (ETL)

Electron transport layers (ETLs) should show a high light transmittance and an appropriate conduction band energy level that is slightly lower than that of the inorganic $CsPbBr_3$ perovskite film, which favors electron injection from the absorber layer to

ETL. In parallel, an ETL also serves as the hole block layer to effectively impede hole transfer to the FTO electrode because of a large gap between the valence band maximum (VBM) of $CsPbBr_3$ and the VBM of ETL. Usually, the choice of ETL materials (Figure 4) includes inorganic metal oxide materials ($TiO_2$, ZnO, $SnO_2$, $WO_3$ and so on)[74-77] and organic carbon-base materials (PCBM, $C_{60}$).[78]

The $TiO_2$ film shows a high crystallinity after annealing at high temperatures (over 450 °C) and can be fabricated as mesoporous structures, which can serve as a scaffold in solution processing and favorable for the nucleation and crystallization of $CsPbBr_3$ films (Figure 4a).[31] Li et al, employed a compact (c-) $TiO_2$ layer with a thickness of 20 nm as ETL by spin-coating precursor solution and treated the c-$TiO_2$ by using a 40 mM aqueous solution of $TiCl_4$ at 70 °C.[60] $CsPbBr_3$ films were deposited by the vapor deposition strategy. Even though the $TiO_2$ has been widely applied in both inorganic and hybrid PSCs, the lower electron mobility (0.1-10 $cm^2\ V^{-1}\ s^{-1}$) of $TiO_2$ layer leads to inefficient charge carrier transport to the transparent electrode, which results in recombination in the PSCs.[75] In parallel, the UV photocatalytic effect of $TiO_2$ films usually causing potential degradation of perovskite films is another issue for the stability of devices.[80]

Besides $TiO_2$ films, $SnO_2$ can also serve as an alternative ETL in $CsPbBr_3$ solar cells because of high electron mobility (240 $cm^2\ V^{-1}\ s^{-1}$), high light transmittance ($E_g$=3.8 eV) and low temperature fabrication (less than 150 °C).[69, 75] You's group and Tang's group employed $SnO_2$ nanoparticles and $SnO_2$ QDs (Figure 4b), respectively, as the ETL in $CsPbBr_3$ solar cells and achieved high efficiencies of 9.81% and 10.6%,

respectively.[51, 69] The annealing temperature of $SnO_2$ nanoparticles and $SnO_2$ QDs were 150 °C (30 min) and 200 °C (60 min) in air, respectively. It is noted that high annealing temperature could damage the quality of the $SnO_2$ layer, resulting in a large number of traps and pinholes in the ETL corroborated by Qi's group.[81] Therefore, $CsPbBr_3$ films on top of $SnO_2$ films need be processed at a lower annealing temperature (250 °C). ZnO possesses a low conduction band of -4.2 eV and a high carrier mobility of 200-300 $cm^2 V^{-1} s^{-1}$, which could improve electron transport from the perovskite to the transparent electrode (Figure 4c). Chen et al. and Zhang et al. employed the ZnO nanoparticles as ETL in $CsPbBr_3$ solar cells and realized a high PCE of 7.78% and 6.81%, respectively.[61, 82] Duan and co-workers recently developed a simplified structure of FTO/$CsPbBr_3$/carbon (Figure 4d). In this structure, the device generated an efficiency of 2.35% without ETL and HTL.[79] Despite the inferior efficiency shown by this structure, the advantages of low-cost and less toxicity are highlighted because no high temperature sintering process is required for the fabrication of ETL and the absence of HTLs leads to cost reduction and avoids usage of toxic solvents needed for HTL material dissolution.

**4.2 Hole transport layer (HTL)**

An ideal hole transport layer (HTL) in PSCs need not only provide hole extraction functionality but also inhibit electron transfer. The highest occupied molecular orbital (HOMO) of 2,2',7,7'-tetrakis (N, N-di-p-methoxyphenylamine)-9,9-spirobifluorene (spiro-OMeTAD) has an energy level matching the VBM of the perovskite materials and has been widely used in PSCs. However, the lower hole mobility of pristine spiro-

OMeTAD films requires the employment of extra additives, for example, lithium bis(trifluoromethanesulfonyl) imide salt (LiTFSI) and 4-tert-butylpyridine (TBP).[83] Poly(triaryl)amine (PTAA) is another ideal candidate as HTL due to its higher carrier mobility (≈1~10×$10^{-2}$ $cm^2$ $V^{-1}$ $S^{-1}$, determined from the field-effect transistor measurements). Copper phthalocyanine (CuPc), as a p-type semiconductor material, also can be used as HTL. The high mobility of $10^{-3}$-$10^{-2}$ $cm^2$ $V^{-1}$ $S^{-1}$, superior stability (starting degradation above 500 °C in air), and long diffusion length (8~68 nm) ensures effective hole extraction in the devices.[84] $CsPbBr_3$-based PSCs with a CuPc HTL deposited on top of $CsPbBr_3$ layer by thermal evaporation and then carbon paste applied as electrode were devised. The highest efficiency of devices with a CuPc HTL was 8.79% with excellent thermal and humidity stability.[53] Alternatively, quantum dots (QDs) can also serve as HTL to replace the expensive organic-semiconductor materials. For example, Zhou and co-workers employed $Cu_2ZnSnS_4$ (CZTS) QDs as HTL in $CsPbBr_3$ PSCs and obtained an efficiency of 4.84%.[70] However, the energy level mismatch was still an issue leading to high recombination rates at the interface. In parallel, $CsMBr_3$ (M= Sn, Bi, Cu) QDs were also used to decorate $CsPbBr_3$ films to increase hole injection by alleviating the energy level mismatch between the $CsPbBr_3$ film and carbon electrode.[69] In addition, in the inverted structure of $CsPbBr_3$ PSCs, the $CsPbBr_3$ films were deposited on the PEDOT:PSS layers with a configuration of ITO/PEDOT:PSS/$CsPbBr_3$/PCBM/Ag.[85] Because the PEDOT:PSS as HTL is usually annealed at temperatures of less than 150 °C, the high annealing temperature of $CsPbBr_3$ would damage PEDOT:PSS. Therefore, in this inverted device with

PEDOT:PSS, $CsPbBr_3$ could only be treated at a lower annealing temperature around 130 ºC, which resulted in a lower crystallization of the $CsPbBr_3$ film.

**4.3 Carbon electrode**

The high-cost and instability issues of HTLs are still a challenge for upscaling of PSCs, which is one of the requirements for deployment in commercial applications. To overcome this problem, replacement of HTL with a low-cost metal and/or carbon to construct HTL-free PSCs is an attractive alternative. Although gold displays a suitable work function matching perovskite material, the high-cost of gold poses difficulty for commercialization. Alternatively, the price of silver is cheaper than gold; however, it has been reported that silver can diffuse into perovskite, damage the quality of perovskite and cause degradation of devices,[86] and also in some cases, the volatile species as a result of degradation of perovskite films in solar cell devices react with silver electrodes leading to reduced device performance.[87] In this case, carbon is an ideal candidate for PSCs because of its low-cost, high stability and also well-matched work function with the VBM of the perovskite layer. Liang et al. employed carbon paste as the electrode for HTL-free $CsPbBr_3$ PSCs with a structure of FTO/$TiO_2$/$CsPbBr_3$/carbon.[31] In this work, the carbon ink was coated by doctor-blade and annealed at 70 °C for 60 min. The appropriate work function (-5.0 eV) of carbon electrode ensured effective hole extraction and collection, which resulted in an impressive PCE of 6.7%. Surprisingly, the device without any encapsulation could survive in a high relative humidity (RH) of ~90% condition without any degradation for over 2640 h. This strategy shows promising application of $CsPbBr_3$ PSCs with

carbon electrode in humid environment. More recently, Liang et al. also applied carbon paste as the electrode for $CsPb_{1-x}Mn_xI_{1+2x}Br_{2-2x}$ PSCs with a structure of FTO/$TiO_2$/$CsPb_{1-x}Mn_xI_{1+2x}Br_{2-2x}$/carbon, which resulted in a PCE of 7.36% and good stability in ambient.[88] Furthermore, Tong et al. and Duan et al. reported the increased efficiencies of 10.17% and 10.14% for the carbon-based $CsPbBr_3$ PSCs by the vapor deposition and solution methods, respectively.[41, 68] These devices also displayed outstanding stability under both moisture (45% RH, over 2500 h) and thermal conditions (100 °C, over 700 h). At present, the highest efficiency of carbon based $CsPbBr_3$ PSCs is up to 10.91%.[64]

In addition, modification of carbon electrodes is also an effective strategy to increase the performance of carbon-electrode-based $CsPbBr_3$ PSCs. The work function of carbon electrodes is close to 5 eV,[89] while VBM of $CsPbBr_3$ is located at approximately 5.6 eV below vacuum level. Such a large energy mismatch at the interface of $CsPbBr_3$/carbon indicates that there is still room to further optimize $CsPbBr_3$ based solar cells to achieve higher performance. Ding et al. introduced the PtNi alloy nanowires (NWs) into the carbon ink to control the work function of carbon electrodes.[90] From ultraviolet photoelectron spectroscopy (UPS) analyses, work function values of 5.0, 5.1, 5.3, 5.4, and 5.5 eV were extracted on carbon electrodes with PtNi doped (from 0 to 7 wt%) into the commercial carbon ink. The highest efficiency of device was up to 7.17% with 3 wt% PtNi NWs.

**4.4 Compositional engineering**

To achieve high efficienciesin$CsPbBr_3$ solar cells, the compositional engineering

strategy that is based on incorporation of A-site, B-site or C-site ionic additives has been shown to be effective. Compositional engineering improves not only the quality of perovskite thin films, but also offers additional benefits of defect healing, energy levels tunability, and structural stability.[65, 67] Since we know, the ionic radius of $Li^+$(0.76 Å), $Na^+$ (1.02 Å), $K^+$(1.38 Å) and $Rb^+$(1.52 Å) are smaller than $Cs^+$ (1.67 Å).[65] Li and co-workers found that partial substitution of A-site cations by smaller cations, for example, alkali metal cations could realize the contraction effect of $CsPbBr_3$ lattice volume.[65] Furthermore, the optical bandgap was also reduced after A-site doping, which could alleviate the energy barrier between $TiO_2$ and $CsPbBr_3$. As a result, a high efficiency of 9.86% for $Cs_{0.91}Rb_{0.09}PbBr_3$, 8.61% for $Cs_{0.92}K_{0.08}PbBr_3$, 8.31% for $Cs_{0.94}Na_{0.06}PbBr_3$ and 7.87% for $Cs_{0.98}Li_{0.02}PbBr_3$ in an HTL-free structure.[65] Additionally, Duan et al. developed a B-site doping method by introducing lanthanide ions into perovskite films.[68] This substitution of $Pb^{2+}$ sites by $Ln^{3+}$ ions could significantly increase crystal size, prolong the carrier lifetime and reduce charge recombination in $CsPbBr_3$ films. An impressive PCE of 10.14% for $CsPb_{0.97}Sm_{0.03}Br_3$ was obtained in the HTL-free PSCs. In parallel, Yin's group proposed a strategy to control the phase transition from orthorhombic to cubic phase by $PbCl_2$ treatment.[91] In this case, chlorine incorporation could serve as an interfacial modifier to increase electron extraction rate. The cubic $CsPbBr_3$ (Cl) phase device showed an efficiency of 6.21% with spiro-OMeTAD as HTL.

**4.5 Interface engineering**

In addition to the light harvesting functionality, $CsPbBr_3$ can also serve as an

interface layer in hybrid organic-inorganic PSCs to passivate the interface, lower the energy barrier, and improve carrier injection (Figure 5).[72, 92, 93] For example, Zai et al. demonstrated the modification of the FAMAPbIBr based hybrid perovskite layer by incorporation of $CsPbBr_3$ nanocrystals (NCs).[71] The incorporated $CsPbBr_3$ NCs could reduce the defect density in the FAMAPbIBr perovskite film and improve the energy level alignment at the interface, which resulted in improvement of carrier extraction and high solar cell efficiencies. A high efficiency of 20.56% was achieved after employing this modification strategy, which is higher than the pristine PSCs with an average PCE of 17.95%. In a follow-up work, Gao and co-workers also investigated the formation of hybrid perovskite films by incorporation of $CsPbBr_3$ nanoparticles (NPs).[73] In this work, the authors found that the $CsPbBr_3$ NPs played a role as nucleation centers, which could slow down the formation speed of the $Cs_{1-y}MA_yPbI_{3-x}Br_x$ absorption layer and passivate the film at the same time. A champion PCE of 20.46% was obtained with 2% $CsPbBr_3$ NPs, and the devices maintained 80% of the initial PCE for more than 500 h under 40% RH.

## 5. Stability.

In addition to efficiency, stability is another important parameter for PSCs to move forward towards commercialization. Stability is affected by intrinsic properties such as phase transition, interfacial ionic diffusion within devices or by external environmental conditions, for example, water, light illumination and elevated temperature.[108]

### 5.1 Humidity stability

Hybrid organic-inorganic perovskite materials are sensitive to water and can be decomposed quickly in moisture environment. By substituting partially $MA^+$ or $FA^+$ by $Cs^+$, the fast decomposition can be alleviated. However, hybrid PSCs still suffer from poor stability when exposed to a high humidity environment for an extended period of time. In contrast, inorganic PSCs exhibit an outstanding stability in high humidity as presented in Figure 6. Liang et al. was the first to report an all inorganic $CsPbBr_3$ PSCs by using carbon electrodes. The devices showed almost no performance degradation in high humid air (90-95% RH) for more than 2640 h (Figure 6a).[31] The XRD diffraction patterns of the $CsPbBr_3$ films before and after exposure to humid environment for over 15 days showed no significant changes (Figure 6b-c). Duan et al. also found that the carbon-electrode based $CsPbBr_3$ solar cells could also keep 87 % of their initial PCE under high moisture conditions (RH~90%).[40] However, compared to case with the carbon electrode without HTL, the $CsPbBr_3$ solar cells with HTM show inferior stability because spiro-OMeTAD and other HTLs are sensitive to water. Liu et al. and Li et al. showed the $CsPbBr_3$ solar cells with a configuration of FTO/$TiO_2$/$SnO_2$/$CsPbBr_3$/CuPc/Carbon (Figure 6d) and FTO/$TiO_2$/$CsPbBr_3$/spiro-OMeTAD/Ag (Figure 6e).[53, 60] The PCE of the device decreased by 10% after 1000 h of exposure to an environment with a relatively humidity (RH) of ~45%, which confirms the superior stability performance of $CsPbBr_3$ PSCs compared to the OIH-PSCs.[10, 19] When the organic HTL is replaced by the inorganic HTL such as $NiO_x$, the moisture stability can be further improved significantly. Yuan and co-workers investigated $NiO_x$ as HTL in $CsPbBr_3$ solar cells and found that the devices not only

showed a high PCE above 10.26%, but also exhibited high stability under the conditions with a RH of 80% (Figure 6f).[105]

**5.2 Thermal stability**

The devices can suffer from thermal degradation during operation and storage (Figure 7). Therefore, thermal stability is another important aspect to be considered. Commercial silicon modules need to operate successfully at an average temperature of 85 °C because such high working temperatures can be often reached in summer or in some regions with high solar irradiance.[109] Usually, inorganic $CsPbBr_3$ films are annealed at high temperatures of 250-350 °C to achieve high crystallinity. The decomposition or mass loss temperature of $CsPbBr_3$ is higher than 350 °C.[96] Thus, $CsPbBr_3$ does not decompose at relatively low temperatures (<85 °C). In contrast, hybrid organic-inorganic perovskite materials, e.g., MA or FA based perovskite films will decompose slowly at such temperatures (<85 °C). It is worth noting that organic HTLs in devices may also degrade at such temperatures (>85 °C). Yin's group designed a comparative experiment by using $CsPbBr_3$ and $MAPbI_3$ based solar cells with a configuration of FTO/$TiO_2$/perovskite/spiro-OMeTAD/Ag (Figure 7d).[91] The samples were kept at 50 °C in a glove box to eliminate the influences from humidity. The $CsPbBr_3$ based devices presented a better thermal stability and maintained 80% of the initial efficiency for 300 h. By contrast, the hybrid $MAPbI_3$ based samples decomposed rapidly at a faster decomposition rate. In addition, the configuration with CuPc and $CsSnBr_3$ QDs as HTL also exhibited excellent thermal stability (Figure 7e and 7f), which retained 80% of their initial performance for 1000 h.[69, 84] For carbon-electrode

based $CsPbBr_3$ solar cells, an outstanding thermal stability is often obtained because of absence of organic HTL and lack of in-diffusion of metal atoms (or ions) in the case when a metal contact (e.g. Au, Ag) is used. For example, Jin, Liang and co-workers reported that a $CsPbBr_3$/carbon based PSC exhibited no degradation at a high temperature of 100 °C in high-humidity environment (90 ~ 95% RH, 25 °C) without encapsulation for 840 h (Figure 7a).[31] In parallel, Qi, Jiang and coworkers also displayed a carbon-electrode based $CsPbBr_3$ devices that was stored in a heated environment at a constant temperature of 100 °C.[41] The PCE of the device dropped to approximately 85% of the original PCE (700 h at 100 °C and ~45% RH) (Figure 7b).[41] In another study, the $Sm^{3+}$ doped $CsPbBr_3$ solar cell devices showed almost no thermal degradation for 60 days at 80 °C and 0% RH (Figure 7c).[68] The analyses of Figures 6 and 7 have indicated that the combination of carbon electrodes with $CsPbBr_3$ perovskites can lead to superior stability in high humidity conditions (e.g., 2500 h at 90 ~ 95% RH; Figure 6a) and elevated temperatures (e.g., 840 h at 100 °C; Figure 7a), which are substantially better than organic-inorganic hybrid counterparts (e.g., ~480 h at 90 ~ 95% RH and 25 °C for Figure 6a; less than 100 h at 100 °C for Figure 7a; ~200 h at 70~80% RH and 100 °C for Figure 7e). However, it was noted that the thermal stability of carbon based $CsPbBr_3$ PSCs (e.g., 840 h, Figure 7a; 14 days, Figure 6f) was still poorer than the humidity stability (e.g., 2640 h, Figure 6a; 40 days, Figure 7f), because the binding properties of polymer binders in the carbon paste might be easily damaged at such high temperatures, which affected the conductivity of carbon electrode and the efficiency of these devices.

Inorganic $CsPbBr_3$ solar cells have better storage stability against moisture and thermal degradation. However, the devices need to be studied under continuous light illumination with maximum power point tracking (MPPT).[110] Currently, there are only two reports on the operational stability employing $CsPbBr_3$. Kulbak and co-workers reported that the $CsPbBr_3$ solar cells with HTL and displayed a much slower and smaller decay (~13%) after 5-hour continuous illumination at an applied bias close to the initial maximum power point (@1 V, Figure 8a).[96] Zhao et al. reported carbon-electrode based $CsPbBr_3$ solar cells under AM 1.5G sun illumination at maximum power point tracking (@1.413 V, Figure 8b). The PCE of device decreased by 20% of its initial efficiency after 100 h.[69] More details about the solar cell operation stability behavior can be found in Figure 8b and ref 69. Despite the advantages of shelf-stability, more operational stability profiles are important to be investigated for moving $CsPbBr_3$ photovoltaic technology from laboratory-scale to industrial-scale fabrication. Operational stability of $CsPbBr_3$ is an essential consideration to evaluate its competitiveness with the current state-of-the-art organic-inorganic mixed PSCs as well as other PV technologies (e.g., Si, CdTe, CIGS).

## 6. Summary and outlook

The central focus of our review is to analyze recent advances of $CsPbBr_3$ PSCs (Table 1) with emphasis on the fabrication methods as well as device architectures relating to their performance and stability. Investigation of $CsPbBr_3$ materials for sun energy harvesting applications was triggered by the fact that (i) organic cations (e.g.,

$MA^+$, $FA^+$) containing PSCs have shown to degrade at ~85 $^oC$, which corresponds to a typical solar cell operation temperature;[2, 12, 111-113] (ii) volatile organic components that sublime from the crystal structure has been reported;[13, 14, 114, 115] (iii) hydrophilic organic groups lead to moisture induced degradation;[116-118] (iii) Br halide based perovskites show better stability when compared to those based on iodine;[13, 14, 114, 115, 119, 120] (iv) although $CsPbI_3$ has a more appropriate bandgap (~1.73 eV), the material transitions to the yellow, insulating, non-perovskite δ-phase at temperatures below 315 $^oC$;[28, 35, 120] (v) structural simplicity and relatively easy synthesis of $CsPbBr_3$.[12, 35, 41, 50, 59, 68, 121] Since the first $CsPbBr_3$-based PSCs with PCEs up to 5.95% were reported in 2015,[52] worldwide research efforts culminated in several state-of-the-art $CsPbBr_3$-based PSCs architectures. In particular, the device structure of FTO/$SnO_2$ QDs ETL/$CsPbBr_3$/$CsSnBr_3$ HTL/carbon can achieve 10.6% PCE with 7.8 mA $cm^{-2}$ $J_{sc}$, 1.61 V $V_{oc}$, and 84.4% FF.[69] This work also provides the realistic operational stability at MPP tracking for 200 h under AM 1.5G sun illumination. Although further research efforts are needed to demonstrate long-term operational stability, $CsPbBr_3$ PSCs are promising and show negligible degradation under humid ambient (20-95% RH) and/or (heat 50-100$^oC$) for over three months without encapsulation.[31]

Despite the advantages of stability and expectation that PCE can be further enhanced in $CsPbBr_3$ PSCs, further major steps of advancing the $CsPbBr_3$ photovoltaic technology from laboratory-scale to industrial-scale fabrication is an essential consideration in order to be competitive compared to the current state-of-the-art organic-inorganic mixed PSCs as well as other PV technologies (e.g., Si, CdTe, CIGS).

Three major aspects to be considered in $CsPbBr_3$ PSC research are (1) PSC fabrication processes must be of low-cost, applicable to large areas, compatible with high throughput and reproducibility; (2) further research efforts are needed to demonstrate the long-term operational stability; and (3) low toxicity. The optimal bandgap for a single-junction solar cells is between 1.1 and 1.4 eV according to the Shockley-Queisser efficiency limit (S-Q limit) model that can lead to a theoretical PCE of ~33%.[35, 122] The bandgap of $CsPbBr_3$ is ~2.3 eV and the S-Q limit model dictates a maximum PCE of ~16.5%. In parallel, the highest $V_{oc}$ of 1.615 V is still significantly lower than the theory calculation value of 1.98 V.[107, 123] The loss of the open circuit voltage of approximately 18% indicates that the energy level alignment can be further improved. One of the advantages of the $CsPbBr_3$ bandgap is the application in multijunction solar cells with PSCs, silicon solar cells or CIGS solar cells.[50, 124] Another outstanding property of $CsPbBr_3$ is the high $V_{oc}$ that can minimize the number of serial connections when considering solar module design. A single-junction solar cell is often inadequate for application purposes on the basis of reported MPP voltage (< 1.6 V) and current (< ~10 mA $cm^{-2}$) in Table 1. Hence, solar module design and fabrication need be devised to meet the voltage and current requirements for targeted niche applications.[125-129] At present, there are no studies on large-scale solar module level employing $CsPbBr_3$ perovskite and the majority of the reported $CsPbBr_3$ PCEs (Table 1) were obtained only on relatively small active areas (< 1 $cm^2$).[53] As comparison, substantial progress has been made in the fabrication of large area organic-inorganic hybrid PSCs and it is becoming a standard to demonstrate PSCs and modules

with total areas larger than 10 $cm^2$.[125] Therefore, keeping in mind commercialization, more efforts are needed in the development of fabrication processes aiming at large-area $CsPbBr_3$ PSCs with high PCE, high-throughput, and minimum batch-to-batch variations. Spin-coating, chemical vapor deposition (CVD), vacuum-based deposition methods were mainly employed for fabricating $CsPbBr_3$ films. Because of the low solubility of CsBr in aprotic solvents, a one-step solution processing method is challenging.[51] Alternatively, two-step solution processing as well as vacuum- and CVD-based deposition have been successful, which are also viable ways for upscaling of $CsPbBr_3$ perovskite films. The formation and co-existence of additional phases of $CsPb_2Br_5$ (Figure 1c; 2D structure with an indirect bandgap of ~3.1 eV)[130] and $Cs_4PbBr_6$ (Figure 1c; 0D structure with an direct bandgap of ~3.95 eV)[58, 131] are often discussed,[19, 53, 59] but further in-depth fundamental investigation is needed to understand their influences on device performance and stability.[60] It has been proposed that phase transitions in inorganic perovskites can be also applied for niche applications such as thermochromic smart windows.[124]

The $CsPbBr_3$ atomic and electronic structures were described by surface science techniques corroborated by density functional theory (DFT) calculations.[132-136] Furthermore, theoretical investigations of point defects and grain boundary induced trap states in $CsPbBr_3$ were reported to lead to shallow trap states within the bandgap demonstrating the superior electronic properties or defect-tolerance property of $CsPbBr_3$.[133, 137-139] Experimentally, efforts have been made to characterize the grain boundaries in $CsPbBr_3$ by electron microscopy techniques[138, 140, 141] For example,

Mishra et al. determined the atomic structures of grain boundaries in $CsPbBr_3$ perovskite nanocrystals by scanning transmission electron microscopy-annular dark field (STEM-HAADF) imaging combined with DFT modeling[138] Grain boundary and Ruddlesden-Popper planar defects of Br-terminated and Br-deficient $CsPbBr_3$ were identified. The Br-terminated type grain boundary defect occurred the most (19 out of 42 analyzed). The other typical planar defect analyzed is the RP planar fault, which consists of two CsBr layers stacked between two $CsPbBr_3$ domains. The RP planar faults propagate along the (010) and (100) planes forming a 90° steps at each intersection. Further examination of the band diagrams across the grain boundary reveals that neither Br-terminated nor RP planar faults induce deep defect levels in the bandgap. However, the Br-deficient defects associated with the presence of Pb dangling bonds or Pb-Pb bonds were identified to lead to deep trap levels.[138] Therefore, passivation of defective $CsPbBr_3$ surfaces is an important consideration for further boosting PCEs.[142-144] On the basis of Table 1, no passivation engineering has been applied on $CsPbBr_3$ PSCs, and this topic certainly warrants further investigation.

Long-term stability (>20 years as has been achieved in the case of Si photovoltaic technology) is a second major consideration, which is still a grand challenge for both organic-inorganic hybrid and inorganic PSCs.[2, 111, 112, 145] In particular, $CsPbBr_3$ perovskite stability under thermal-stress and light testing conditions is important for solar cell-operation following the industry-relevant protocols.[146] Based on our review (Section 5), $CsPbBr_3$ shows outstanding improvements regarding thermal and moisture stability when compared to organic-inorganic hybrid perovskites, but it is still far from

the thresholds for long-term-stability considerations. Furthermore, currently there is only one work reporting the realistic operational stability at MPP tracking for 200 h under AM1.5G sun illumination showing a decay of 80% of its initial PCE in 100 h.[69] Interface related chemical reactions at perovskite/selective contacts have been proposed as one of the causes for the degradation of overall PSC performance.[147-149] In addition, physico-chemical degradation processes of selective contacts and electrodes are important to be considered when investigating operational stability of the whole $CsPbBr_3$ PSC (i.e., the PCE decay is a result from the degradation of the perovskite layer and its adjacent layers of selective contacts and electrodes).[2, 81, 113, 150] In comparison with the organic-inorganic hybrid perovskites, the high temperature tolerance of $CsPbBr_3$ widens the material choice (selective contacts and/or electrodes) as well as its processing temperatures for subsequent depositions onto $CsPbBr_3$ films. As discussed in Section 5, the carbon electrode layer on $CsPbBr_3$ PSCs helps prolong stability under continuous light illumination, due to the hydrophobic properties of the carbon electrode. In addition, the low-cost of carbon paste is attractive for industry and academia.

Similar with organic-inorganic hybrid PSCs, toxicity of $Pb^{2+}$ is a third major drawback of high-efficiency perovskite-based solar cells that concerns investors and consumers.[126] Therefore, great efforts are being made to identify environmentally friendly lead-free perovskite structures. PSCs based on $CsSnBr_3$ have been demonstrated recently as a promising Pb-free alternative, but more research efforts are still needed to optimize their film quality as well as chemical stability of $Sn^{2+}$.[151-153]

Regarding the latter issue, composition engineering (i.e., Sn-Ge alloy) and native-oxide passivation layer have been proposed as promising strategies.[154] Double perovskites such as $Cs_2AgBiBr_6$ are also considered as promising Pb-free alternative, but current reported PCEs are much lower.[155] Encapsulation is important for all PV cells but is particularly important for the PSCs, which not only helps prevent the contact with moisture and oxygen, but also helps prevent the leakage of lead to ambient.[25] Encapsulation technology is expected to play an important role in the development of large scale $CsPbBr_3$ perovskite solar modules. Overall, $CsPbBr_3$ PSCs have shown tremendous progress in just four years exhibiting a great potential for solar cell applications. The next few years of worldwide research efforts are foreseen to produce further important findings and strategies of new processes and device architectures leading to more efficient and non-toxic perovskite solar modules with enhanced stability.

**Acknowledgements**

This work was supported by funding from the Energy Materials and Surface Sciences Unit of the Okinawa Institute of Science and Technology Graduate University, the OIST R&D Cluster Research Program, the OIST Proof of Concept (POC) Program, and JSPS KAKENHI Grant Number JP18K05266.

Received: ((will be filled in by the editorial staff))

Revised: ((will be filled in by the editorial staff))

Published online: ((will be filled in by the editorial staff))

**Reference**


[1] Y. Zhao, K. Zhu, *Chem. Soc. Rev.* **2016**, *45*, 655-689.

[2] L. K.Ono, Y. B. Qi, S. F. Liu, *Joule* **2018**, *2*, 1961-1990.

[3] S. R. Raga, Y. Jiang, L. K. Ono, Y. B. Qi, *Energy Technology* **2017**, *5*, 1750-1761.

[4] Z. Song, G. Tong, H. Li, G. Li, S. Ma, S. Yu, Q. Liu, Y. Jiang, *Nanotechnology* **2018**, *29*, 025401.

[5] J. Lu, X. Sheng, G. Tong, Z. Yu, X. Sun, L. Yu, X. Xu, J. Wang, J. Xu, Y. Shi, K. Chen, *Adv. Mater.* **2017**, *29*, 1700400.

[6] A. Kojima, K. Teshima, Y. Shirai, T. Miyasaka, *J. Am. Chem. Soc.* **2009**, *131*, 6050-6051.

[7] https://www.nrel.gov/pv/assets/pdfs/best-research-cell-efficiencies-190416.pdf (2019).

[8] M. A. Green, Y. Hishikawa, E. D. Dunlop, D. H. Levi, J. HohlEbinger, M. Yoshita, A. W. Y. Ho-Baillie, *Prog. Photovoltaics Res. Appl.* **2019**, *27*, 3-12.

[9] L. Qiu, S. He, Y. Jiang, D.-Y. Son, L. K. Ono, Z. Liu, T. Kim, T. Bouloumis, S. Kazaoui, Y. B. Qi, *J. Mater. Chem. A* **2019**, *7*, 6920-6929.

[10] G. Tong, X. Geng, Y. Yu, L. Yu, J. Xu, Y. Jiang, Y. Sheng, Y. Shi, K. Chen, *RSC Adv.* **2017**, *7*, 18224- 18230.

[11] D. Shan, G. Tong, Y. Cao, M. Tang, J. Xu, L. Yu, K. Chen, *Nanoscale Res Lett* **2019**, *14*, 208.

[12] L. K. Ono, E. J. Juarez-Perez, Y. B. Qi, *ACS Appl. Mater. Interfaces* **2017**, *9*, 30197- 30246.

[13] E. J. Juarez-Perez, Z. Hawash, S. R. Raga, L. K. Ono, Y. B. Qi, *Energy Environ. Sci.* **2016**, *9*, 3406-3410.

[14] E. J. Juarez-Perez, L. K. Ono, M. Maeda, Y. Jiang, Z. Hawash, Y. B. Qi, *J. Mater. Chem. A* **2018**, *6*, 9604-9612.

[15] B. Mi, H. Li, Z. Song, G. Zhao, G. Tong, Y. Jiang. *Nano* **2017**, 12, 1750150-1750159.

[16] J.-W. Xiao, L. Liu, D. Zhang, N. De Marco, J.-W. Lee, O. Lin, Q. Chen, Y. Yang, *Adv. Energy Mater.* **2017**, *7*, 1700491.

[17] M. Saliba, T. Matsui, J. Y. Seo, K. Domanski, J. P. Correa-Baena, M. K. Nazeeruddin, S. M. Zakeeruddin, W. Tress, A. Abate, A. Hagfeldt, M. Gratzel, *Energy Environ. Sci.* **2016**, *9*, 1989-1997.

[18] Y. Jiang, M. R. Leyden, L. Qiu, S. Wang, L. K. Ono, Z. Wu, E. J. Juarez-Perez, Y. B. Qi, *Adv. Funct. Mater.* **2018**, *28*, 1703835.

[19] G. Tong, H. Li, G. Li, T. Zhang, C. Li, L. Yu, J. Xu, Y. Jiang, Y. Shi, K. Chen, *Nano Energy* **2018**, *48*, 536-542.

[20] T. Liu, Y. Zhou, Z. Li, L. Zhang, M.-G. Ju, D. Luo, Y. Yang, M. Yang, D. H. Kim, W. Yang, N. P. Padture, M. C. Beard, X. C. Zeng, K. Zhu, Q. Gong, R. Zhu, *Adv. Energy Mater.* **2018**, *8*, 1800232.

[21] T. Niu, J. Lu, R. Munir, J. Li, D. Barrit, X. Zhang, H. Hu, Z. Yang, A. Amassian, K. Zhao, S. F. Liu, *Adv. Mater.* **2018**, *30*, 1706576.

[22] L. Jiang, Z. Wang, M. Li, C. Zhang, Q. Ye, K. Hu, D. Lu, P. Fang, L. Liao, *Adv. Funct. Mater.* **2018**, *28*, 1705875.

[23] Y. Han, S. Meyer, Y. Dkhissi, K. Weber, J. M. Pringle, U. Bach, L. Spiccia, Y.-B. Cheng, *J. Mater. Chem. A* **2015**, *3*, 8139-8147.

[24] H. C. Weerasinghe, Y. Dkhissi, A. D. Scully, R. A. Caruso, Y.-B. Cheng, *Nano Energy* **2015**, *18*, 118-125.

[25] Y. Jiang, L. Qiu, E. J. Juarez-Perez, L. K. Ono, Z. Hu, Z. Liu, Z. Wu, L. Meng, Q. Wang, Y. B. Qi, *Nat. Energy* **2019**, *4*, 585-593.

[26] J. Zhang, G. Hodes, Z. Jin, S. F. Liu, *Angew. Chem. Int. Ed.* **2019**, *58*, 2-25.

[27] C. Dong, X. Han, W. Li, Q. Qiu, J. Wang, *Nano Energy* **2019**, *59*, 553-559.

[28] Y. Wang, T. Zhang, M. Kan, Y. Zhao, *J. Am. Chem. Soc.* **2018**, *140*, 12345-12348.

[29] Y. Wang, M. I. Dar, L. K. Ono, T. Zhang, M. Kan, Y. Li, L. Zhang, X. Wang, Y. Yang, X. Gao,Y. B. Qi, M. Grätzel, Y. Zhao, *Science*, **2019**, *365*, 591-595.

[30] Q. Wang, X. Zhang, Z. Jin, J. Zhang, Z. Gao, Y. Li, S. F. Liu, *ACS Energy Lett.* **2017**, *2*, 1479-1486.

[31] J. Liang, C. Wang, Y. Wang, Z. Xu, Z. Lu, Y. Ma, H. Zhu, Y. Hu, C. Xiao, X. Yi, G. Zhu, H. Lv, L. Ma, T. Chen, Z. Tie, Z. Jin, J. Liu, *J. Am. Chem. Soc.* **2016**, *138*, 15829-15832.

[32] Q. Zeng, X. Zhang, C. Liu, T. Feng, Z. Chen, W. Zhang, W. Zheng, H. Zhang, B. Yang, *Sol. RRL.* **2018**, *3*, 1800239.

[33] K. Wang, Z. Jin, L. Liang, H. Bian, D. Bai, H. Wang, J. Zhang, Q. Wang, S. Liu,

*Nat. Commun.* **2018**, *9*, 4544.

[34] Y. Wang, X. Liu, T. Zhang, X., Wang, M. Kan, J. Shi, Y. Zhao, *Angew. Chem. Int. Ed.* **2019**, DOI: 10.1002/anie.201910800.

[35] Q. Tai, K.-C. Tang, F. Yan, *Energy Environ. Sci.* **2019**,12, 2375-2405.

[36] C. C. Stoumpos, C. D. Malliakas, J. A. Peters, Z. Liu, M. Sebastian, J. Im, T. C. Chasapis, A. C. Wibowo, D. Y. Chung, A. J. Freeman, B. W. Wessels, M. G. Kanatzidis, *Cryst. Growth Des.* **2013**, *13*, 2722-2727.

[37] A. Swarnkar, W. J. Mir, A. Nag, *ACS Energy Lett.* **2018**, *3*, 286-289.

[38] S. Gholipour, A. M. Ali, J.-P. C.-Baena, S.-H. T.-Cruz, F. Tajabadi, W. Tress, N. Taghavinia, M. Grätzel, A. Abate, F. D. Angelis, C. A. Gaggioli, E. Mosconi, A. Hagfeldt, M. Saliba, *Adv. Mat.* **2017**, *29*, 1702005.

[39] P. Teng, X. Han, J. Li, Y. Xu, L. Kang, Y. Wang, Y. Yang, T. Yu, *ACS Appl. Mater. Interfaces* **2018**, *10*, 9541-9546.

[40] J. Duan, Y. Zhao, B. He, and Q. Tang, *Angew. Chem. Int. Ed.* **2018**, *57*, 3787-3791.

[41] G. Tong, T. Chen, H. Li, W. Song, Y. Chang, J. Liu, L. Yu, J. Xu, Y. B. Qi, Y. Jiang, *Sol. RRL* **2019**, *3*, 1900030.

[42] G. Li, H. Wang, Z. Zhu, Y. Chang, T. Zhang, Z. Song, Y. Jiang, *Chem. Commun.* **2016**, *52*, 11296-11299.

[43] F. Palazon, S. Dogan, S. Marras, F. Locardi, I. Nelli, P. Rastogi, M. Ferretti, M. Prato, R. Krahne, L. Manna, *J. Phys. Chem. C* **2017**, *121*, 11956-11961.

[44] H. Zhu, M. T. Trinh, J. Wang, Y. Fu, P. P. Joshi, K. Miyata, S. Jin, X. Y. Zhu,

*Adv. Mater.* **2017**, *29*, 1603072.

[45] D. N. Dirin, I. Cherniukh, S. Yakunin, Y. Shynkarenko, M. V. Kovalenko, *Chem. Mater.* **2016**, *28*, 8470-8474.

[46] M. Kulbak, I. Levine, E. Barak-Kulbak, S. Gupta, A. Zohar, I. Balberg, G. Hodes, D. Cahen, *Adv. Energy Mater.* **2018**, *8*, 1800398.

[47] J. Song, Q. Cui, J. Li, J. Xu, Y. Wang, L. Xu, J. Xue, Y. Dong, T. Tian, H. Sun, H. Zeng, *Adv. Optical Mater.* **2017**, *5*, 1700157.

[48] G. A. Elbaz, D. B. Straus, O. E. Semonin, T. D. Hull, D. W. Paley, P. Kim, J. S. Owen, C. R. Kagan, X. Roy, *Nano Lett.* **2017**, *17*, 1727-1732.

[49] Y. Rakita, N. Kedem, S. Gupta, A. Sadhanala, V. Kalchenko, M. L. Böhm, M. Kulbak, R. H. Friend, D. Cahen, G. Hodes, *Cryst. Growth Des.* **2016**, *16*, 5717-5725.

[50] J. Liang, J. Liu, Z. Jin, *Sol. RRL* **2017**, *1*, 1700086.

[51] P. Wang, X. Zhang, Y. Zhou, Q. Jiang, Q. Ye, Z. Chu, X. Li, X. Yang, Z. Yin, J. You, *Nat. Commun.* **2018**, *9*, 2225.

[52] M. Kulbak, D. Cahen, G. Hodes, *J. Phys. Chem. Lett.* **2015**, *6*, 2452-2456.

[53] X. Liu, X. Tan. Z. Liu, H. Ye, B. Sun, T. Shi, Z. Tang, G. Liao, *Nano Energy* **2019**, *56*, 184-195.

[54] P. Pal, S. Saha, A. Banik, A. Sarkar, K. Biswas, *Chem. Eur. J.* **2018**, *24*, 1811-1815.

[55] L. K. Ono, S. Wang, Y. Kato, S. R. Raga, Y. B. Qi, *Energy Environ. Sci.* **2014**, *7*, 3989-3993.

[56] C. Y. Chen, H. Y. Lin, K. M. Chiang, W. L. Tsai, Y. C. Huang, C. S. Tsao, H. W. Lin, *Adv. Mater.* **2017**, *29*, 1605290.

[57] L. K. Ono, M. R. Leyden, S. Wang, Y. B. Qi, *J. Mater. Chem. A* **2016**, *4*, 6693-6713.

[58] G. Tong, H. Li, Z. Zhu, Y. Zhang, L. Yu, J. Xu, Y. Jiang, *J. Phys. Chem. Lett.* **2018**, *9*, 1592-1599.

[59] G. Tong, H. Li, D. Li, Z. Zhu, E. Xu, G. Li, L. Yu, J. Xu, Y. Jiang, *Small* **2018**, *14*, 1702523.

[60] H. Li, G. Tong, T. Chen, H. Zhu, G. Li, Y. Chang, L. Wang, Y. Jiang *J. Mater. Chem. A* **2018**, *6*, 14255-14261.

[61] W. Chen, J. Zhang, G. Xu, R. Xue, Y. Li, Y. Zhou, J. Hou, Y. Li, *Adv. Mater.* **2018**, *30*, 1800855.

[62] P. Luo, Y. Zhou, S. Zhou, Y. Lu, C. Xu, W. Xia, L. Sun, *Chem. Eng. J.* **2018**, *343*, 146-154.

[63] J. Lei, F. Gao, H. Wang, J. Li, J. Jiang, X. Wu, R. Gao, Z. Yang, S. Liu, *Sol. Energy Mater. Sol. Cells* **2018**, *187*, 1-8.

[64] G. Tong, T. Chen, H. Li, L. Qiu, Z. Liu, Y. Dang, W. Song, L. K. Ono, Y. Jiang, Y. B. Qi, *Nano Energy* **2019**, *65*, 104015.

[65] Y. Li, J. Duan, H. Yuan, Y. Zhao, B. He, Q. Tang, *Sol. RRL* **2019**, *2*, 1800164.

[66] M. R. Linaburg, E. T. McClure, J. D. Majher, P. M. Woodward, *Chem. Mater.* **2017**, *29*, 3507-3514.

[67] Y. Zhao, Y. Wang, J. Duan, X. Yang, Q. Tang, *J. Mater. Chem. A* **2019**, *7*, 6877-

6882.

[68] J. Duan, Y. Zhao, X. Yang, Y. Wang, B. He, Q. Tang, *Adv. Energy Mater.* **2018**, *8*, 1802346.

[69] Y. Zhao, J. Duan, H. Yuan, Y. Wang, X. Yang, B. He, Q. Tang, *Sol. RRL* **2019**, *3*, 1800284.

[70] Z. Zhou, Y. Deng, P. Zhang, D. Kou, W. Zhou, Y. Meng, S. Yuan, S. Wu, *Sol. RRL* **2019**, *3*, 1800354.

[71] H. Zai, C. Zhu, H. Xie, Y. Zhao, C. Shi, Z. Chen, X. Ke, M. Sui, C. Chen, J. Hu, Q. Zhang, Y. Gao, H. Zhou, Y. Li, Q. Chen, *ACS Energy Lett.* **2017**, *3*, 30-38.

[72] C. Chen, Y. Wu, L. Liu, Y. Gao, X. Chen, W. Bi, X. Chen, D. Liu, Q. Dai, H. Song, *Adv. Sci.* **2019**, *6*, 1802046.

[73] Y. Gao, Y. Wu, H. Lu, C. Chen, Y. Liu, X. Bai, L. Yang, W. W. Yu, Q. Dai, Y. Zhang, *Nano Energy* **2019**, *59*, 517-526.

[74] J. P. Correa Baena, L. Steier, W. Tress, M. Saliba, S. Neutzner, T. Matsui, F. Giordano, T. J. Jacobsson, A. R. Srimath Kandada, S. M. Zakeeruddin, A. Petrozza, A. Abate, M. K. Nazeeruddin, M. Grätzel, A. Hagfeldt, *Energy Environ. Sci.* **2015**, *8*, 2928-2934.

[75] W. Q. Wu, D. Chen, R. A. Caruso, Y.-B. Cheng, *J. Mater. Chem. A* **2017**, *5*, 10092-10109.

[76] G. Tong, X. Lan, Z. Song, G. Li, H. Li, L. Yu, J. Xu, Y. Jiang, Y. Sheng, Y. Shi, K. Chen, *Mater. Today Energy* **2017**, *5*, 173-180.

[77] G. Tong, Z. Song, C. Li, Y. Zhao, L. Yu, J. Xu, Y. Jiang, Y. Sheng, Y. Shi, K.

Chen, *RSC Adv.*, **2017**, *7*, 19457-19463.

[78] K. Wojciechowski, T. Leijtens, S. Siprova, C. Schlueter, M. T. Horantner, J. T. Wang, C. Z. Li, A. K. Jen, T. L. Lee, H. J. Snaith, *J. Phys. Chem. Lett.* **2015**, *6*, 2399-2405.

[79] J. Duan, Y. Zhao, B. He, Q. Tang, *Small* **2018**, *14*, 1704443.

[80] S. W. Lee, S. Kim, S. Bae, K. Cho, T. Chung, L. E. Mundt, S. Lee, S. Park, H. Park, M. C. Schubert, S. W. Glunz, Y. Ko, Y. Jun, Y. Kang, H. S. Lee, D. Kim, *Sci. Rep.* **2016**, *6*, 38150.

[81] L. Qiu, Z. Liu, L. K. Ono, Y. Jiang, D.-Y. Son, Z. Hawash, S. He, and Y. B. Qi, *Adv. Funct. Mater.* **2018**, *19*, 1806779.

[82] X. Zhang, Z. Jin, J. Zhang, D. Bai, H. Bian, K. Wang, J. Sun, Q. Wang, S. F. Liu, *ACS Appl. Mater. Interfaces* **2018**, *10*, 7145-7154.

[83] Z. Yu, L. Sun, *Adv. Energy Mater.* **2015**, *5*, 1500213.

[84] Z. Liu, B. Sun, X. Liu, J. Han, H. Ye, T. Shi, Z. Tang, G. Liao, *Nano-Micro Lett.* **2018**, *10*, 34.

[85] S. Y. Luchkin, A. F. Akbulatov, L. A. Frolova, S. A. Tsarev, P. A. Troshin, K. J. Stevenson, *Sol. Energy Mater. Sol. Cells* **2017**, *171*, 205-212.

[86] H. Chen, S. Yang, *J. Mater. Chem. A* **2019**, *7*, 15476-15490.

[87] Y. Kato, L. K. Ono, M. V. Lee, S. Wang, S. R. Raga, Y. B. Qi, *Adv. Mater. Interfaces* **2015**, *2*, 1500195.

[88] J. Liang, Z. Liu, L. Qiu, Z. Hawash, L. Meng, Z. Wu, Y. Jiang, L. K. Ono, Y. B. Qi, *Adv. Energy Mater.* **2018**, *8*, 1800504.

[89] Z. Ku, Y. Rong, M. Xu, T. Liu, H. Han, *Sci. Rep.* **2013**, *3*, 3132.

[90] J. Ding, Y. Zhao, J. Duan, B. He, Q. Tang, *ChemSusChem* **2018**, *11*, 1432-1437.

[91] B. Li, Y. Zhang, L. Zhang, L. Yin, *J. Power Sources* **2017**, *360*, 11-20.

[92] Y. Chen, L. Li, Z. Liu, N. Zhou, Q. Chen, H. Zhou, *Nano Energy* **2017**, *40*, 540-549.

[93] W. Zhou, S. Chen, Y. Zhao, Q. Li, Y. Zhao, R. Fu, D. Yu, P. Gao, Q. Zhao, *Adv. Funct. Mater.* **2019**, *29*, 1809180.

[94] S. Panigrahi, S. Jana, T. Calmeiro, D. Nunes, R. Martins, E. Fortunato, *ACS Nano* **2017**, *11*, 10214-10221.

[95] K. C. Tang, P. You, F. Yan, *Sol. RRL* **2018**, *2*, 1800075.

[96] M. Kulbak, S. Gupta, N. Kedem, I. Levine, T. Bendikov, G. Hodes, D. Cahen, *J. Phys. Chem. Lett.* **2016**, *7*, 167-172.

[97] S. Zhou, R. Tang, H. Li, L. Fu, B. Li, L. Yin, *J. Power Sources*, **2019**, *439*, 227065.

[98] J. Liu, L. Zhu, S. Xiang, Y. Wei, M. Xie, H. Liu, W. Li, H. Chen, *Sustainable Energy Fuels* **2019**, *3*, 184-194.

[99] G. Wang, W. Dong, A. Gurung, K. Chen, F. Wu, Q. He, R. Pathak, Q. Qiao, *J. Power Sources* **2019**, *432*, 48-54.

[100] I. Poli, J. Baker, J. McGettrick, F. De Rossi, S. Eslava, T. Watson, P. J. Cameron, *J. Mater. Chem. A* **2018**, *6*, 18677-18686.

[101] H, Guo, Y, Pei, J, Zhang, C, Cai, K, Zhou, Y, Zhu, *J. Mater. Chem. C* **2019**, *7*, 11234-11243.

[102] Y. Zhang, L. Luo, J. Hua, C. Wang, F. Huang, J. Zhong, Y. Peng, Z. Ku, Y.-b. Cheng, *Materials Science in Semiconductor Processing* **2019**, *98*, 39-43.

[103] T. Chen, G. Tong, E. Xu, H. Li , P. Li, Z. Zhu, J. Tang, Y. B. Qi, Y, Jiang, *J. Mater. Chem. A* **2019**, *7*, 20597 - 20603.

[104] Y. Liu, B. He, J. Duan, Y. Zhao, Y. Ding, M. Tang, H. Chen, Q. Tang, *J. Mater. Chem. A* **2019**, *7*, 12635-12644.

[105] H. Yuan, Y. Zhao, J. Duan, Y. Wang, X. Yang, Q. Tang, *J. Mater. Chem. A* **2018**, *6*, 24324-24329.

[106] X. Li, Y. Tan, H. Lai, S. Li, Y. Chen, S. Li, P. Xu, J. Yang, *ACS Appl. Mater. Interfaces* **2019**, *11*, 29746-29752.

[107] J. Duan, Y. Zhao, Y. Wang, X. Yang, Q. Tang, *Angew. Chem. Int. Ed.* **2019**, DOI: 10.1002/anie.201910843.

[108] Z. Wu, Z. Liu, Z. Hu, Z. Hawash, L. Qiu, Y. Jiang, L. K. Ono, Y. B. Qi, *Adv. Mater.* **2019**, *31*, 1804284.

[109] R. J. Sutton, Giles. E. E, L. Miranda, E. S. Parrott, B. A. Kamino, J. B. Patel, M. T. Hörantner, M. B. Johnston, A. A. Haghighirad, D. T. Moore, H. J. Snaith, *Adv. Energy Mater.* **2016**, *6*, 1502458.

[110] Z. Liu, L. Qiu, E. J. Juarez-Perez, Z. Hawash, T. Kim, Y. Jiang, Z. Wu, S. R. Raga, L. K. Ono, S. F. Liu, Y. B. Qi, *Nat. Commun.* **2018**, *9*, 3880.

[111] S.-H. Turren-Cruz, A. Hagfeldt, M. Saliba, *Science* **2018**, *362*, 449-453.

[112] P. Holzhey, P. Yadav, S.-H. Turren-Cruz, M. Grätzel, A. Hagfeldt, M. Saliba, *Materials Today* **2018**, DOI: 10.1016/j.mattod.2018.10.017

[113] L. K. Ono, Y. B. Qi, *J. Phys. D. Appl. Phys.* **2018**, *51*, 093001.

[114] E. J. Juarez-Perez, L. K. Ono, Y. B. Qi, *J. Mater. Chem. A* **2019**, *7*, 16912-16919.

[115] E. J. Juarez-Perez, L. K. Ono, I. Uriarte, E. J. Cocinero, Y. B. Qi, *ACS Appl. Mater. Interfaces* **2019**, *11*, 12586-12593.

[116] Q. Wang, B. Chen, Y. Liu, Y. Deng, Y. Bai, Q. Dong, J. Huang, *Energy Environ. Sci.* **2017**, *10*, 516-522.

[117] J. Huang, S. Tan, P. D. Lund, H. Zhou, *Energy Environ. Sci.* **2017**, *10*, 2284-2311.

[118] J. Yang, B. D. Siempelkamp, D. Liu, T. L. Kelly, *ACS Nano* **2015**, *9*, 1955-1963.

[119] S. Wang, Y. Jiang, E. J. Juarez-Perez, L. K. Ono, Y. B. Qi, *Nat. Energy* **2016**, *2*, 16195.

[120] R. G. Wilks, M. Bär, *Nat. Energy* **2017**, *2,* 16204.

[121] M. Saliba, *Adv. Energy Mater.* **2019**, *9*, 1803754.

[122] S. Ruhle, *Solar Energy*, **2016**, *130*, 139-147.

[123] J. Duan, H. Xu, W. E. I. Sha, Y. Zhao, Y. Wang, X. Yang, Q. Tang, *J. Mater. Chem. A* **2019**, *7*, 21036-21068.

[124] A. Ho-Baillie, M. Zhang, C. F. J. Lau, F.-J. Ma, S. Huang, *Joule* **2019**, *3*, 938-955.

[125] S. He, L. Qiu, D.-Y. Son, Z. Liu, E. J. Juarez-Perez, L. K. Ono, C. Stecker, Y. B. Qi, *ACS Energy Lett.* **2019**, *4*, 2032-2039.

[126] L. Qiu, L. K. Ono, Y. B. Qi, *Mater. Today Energy* **2018**, *7*, 169-189.

[127] L. Gao, L. Chen, S. Huang, X. Li, G. Yang, *ACS Appl. Energy Mater.* **2019**, *2*,

3851-3859.

[128] Y. Rong, Y. Hu, A. Mei, H. Tan, M. I. Saidaminov, S. I. Seok, M. D. McGehee, E. H. Sargent, H. Han, *Science* **2018**, *361,* 6408.

[129] B. Wilkinson, N. L. Chang, M. A. Green, A. W. Y. Ho-Baillie, *Prog Photovolt Res Appl.* **2018**, *26*, 659-674.

[130] I. Dursun, M. D. Bastiani, B. Turedi, B. Alamer, A. Shkurenko, J. Yin, A.M. El-Zohry, I. Gereige, A. AlSaggaf, O.F. Mohammed, M. Eddaoudi, O.M. Bakr, *ChemSusChem* **2017**, *10*, 3746-3749.

[131] Z. Gan, F. Zheng, W. Mao, C. Zhou, W. Chen, U. Bach, P. Tapping, T. W. Kee, J. A. Davis, B. Jia, X. Wen, *Nanoscale* **2019**, *11*, 14676-14683.

[132] B. Akbali, G. Topcu, T. Guner, M. Ozcan, M. M. Demir, H. Sahin, *Phys. Rev. Materials* **2018**, *2*, 034601.

[133] Y. Guo, Q. Wang, W. A. Saidi, *J. Phys. Chem. C* **2017**, *121*, 1715-1722.

[134] J. Endres, D. A. Egger, M. Kulbak, R. A. Kerner, L. Zhao, S. H. Silver, G. Hodes, B. P. Rand, D. Cahen, L. Kronik, A. Kahn, *J. Phys. Chem. Lett.* **2016**, *7*, 2722-2729.

[135] J. Endres, M. Kulbak, L. Zhao, B. P. Rand, D. Cahen, G. Hodes, A. Kahn, *J. Appl. Phys.* **2017**, *121*, 035304.

[136] P. Schulz, *ACS Energy Lett.* **2018**, *3*, 1287-1293.

[137] J. Kang, L. W. Wang, *J. Phys. Chem. Lett.* **2017**, *8*, 489-493.

[138] A. S. Thind, G. Luo, J. A. Hachtel, M. V. Morrell, S. B. Cho, A. Y. Borisevich, J. C. Idrobo, Y. Xing, R. Mishra, *Adv Mater* **2019**, *31*, 1805047.

[139] L. K. Ono, S. Liu, Y. B. Qi, *Angew.Chem. Int. Ed.* **2019**, DOI: 10.1002/anie.201905521.

[140] Y. Yu, D. Zhang, P. Yang, *Nano Lett.* **2017**, *17*, 5489-5494.

[141] Y. Yu, D. Zhang, C. Kisielowski, L. Dou, N. Kornienko, Y. Bekenstein, A. B. Wong, A. P. Alivisatos, P. Yang, *Nano Lett.* **2016**, *16*, 7530-7535.

[142] D. Meggiolaro, E. Mosconi, F. De Angelis, *ACS Energy Lett.* **2019**, *4*, 779-785.

[143] E. H. Jung, N. J. Jeon, E. Y. Park, C. S. Moon, T. J. Shin, T. Y. Yang, J. H. Noh, J. Seo, *Nature* **2019**, *567*, 511-515.

[144] Q. Jiang, Y. Zhao, X. Zhang, X. Yang, Y. Chen, Z. Chu, Q. Ye, X. Li, Z. Yin, J. You, *Nat. Photonics* **2019**, *13*, 460-466.

[145] M. Saliba, *Science* **2018**, *359*, 388-389.

[146] P. Holzhey, M. Saliba, *J. Mater. Chem. A* **2018**, *6*, 21794-21808.

[147] C.-X. Qian, Z.-Y. Deng, K. Yang, J. Feng, M.-Z. Wang, Z. Yang, S. Liu, H.-J. Feng, *Appl. Phys. Lett* **2018**, *112*, 093901.

[148] A. Fakharuddin, L. Schmidt-Mende, G. Garcia-Belmonte, R. Jose, I. Mora-Sero, *Adv. Energy Mater.* **2017**, *7*, 1700623.

[149] J. Shi, X. Xu, D. Li, Q. Meng, *Small* **2015**, *11*, 2472.

[150] Z. Hawash, L. K. Ono, Y. B. Qi, *Adv. Mater. Interfaces* **2018**, *5*, 1700623.

[151] S. Gupta, T. Bendikov, G. Hodes, D. Cahen, *ACS Energy Lett.* **2016**, *1*, 1028-1033.

[152] B. Li, R. Long, Y. Xia, Q. Mi, *Angew.Chem. Int. Ed.* **2018**, *57*, 13154-13158.

[153] J. Jiang, C. K. Onwudinanti, R. A. Hatton, P. A. Bobbert, S. Tao, *J. Phys. Chem.*

*C* **2018**, *122*, 17660-17667.

[154] M. Chen, M. G. Ju, H. F. Garces, A. D. Carl, L. K. Ono, Z. Hawash, Y. Zhang, T. Shen, Y. B. Qi, R. L. Grimm, D. Pacifici, X. C. Zeng, Y. Zhou, N. P. Padture, *Nat. Commun.* **2019**, *10*, 16.

[155] Z. Xiao, W. Meng, J. Wang, D. B. Mitzi, Y. Yan, *Mater. Horiz.* **2017**, *4*, 206-216.

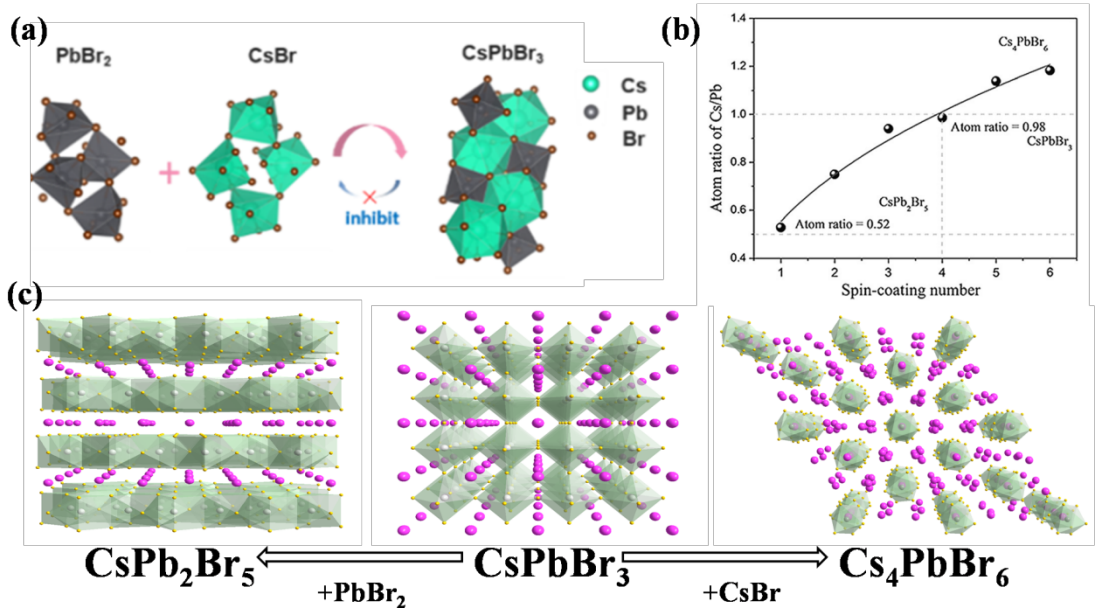


**Figure 1.** (a) Schematic crystal structures of CsBr, $PbBr_2$ and formation of inorganic perovskite $CsPbBr_3$. Reprinted with permission from ref. [39]. Copyright 2018 American Chemical Society. (b) Atomic Cs/Pb ratios determined by EDS inferring the different phases by the multi-step spin-coating by increasing deposition cycles of CsBr solution. Reprinted with permission from ref. [40]. Copyright 2018 WILEY-VCH Verlag GmbH & Co. KGaA, Weinheim. (c) Schematic crystal structures and formation of inorganic perovskite derivative phases ($CsPb_2Br_5$ and $Cs_4PbBr_6$). Reprinted with permission from ref. [41]. Copyright 2019 WILEY-VCH Verlag GmbH & Co. KGaA, Weinheim.

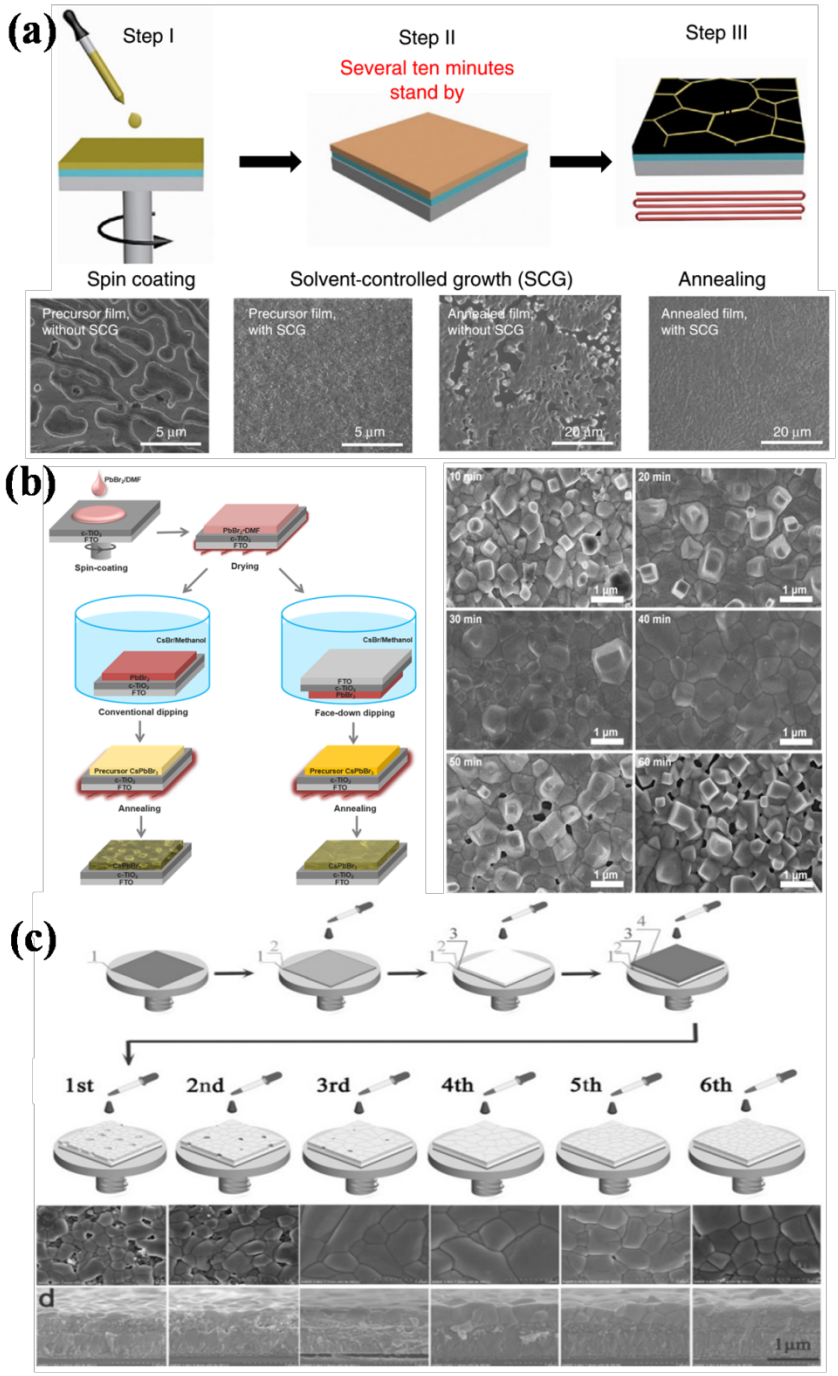


**Figure 2.** (a) Schematic diagram showing the one-step solution method and top-view SEM images of an inorganic $CsPbBr_3$ film. Reprinted with permission from ref. [51]. Copyright 2018 Nature Publishing Group. (b) Schematic diagram showing the two-step solution method via dipping and top-view SEM images of an inorganic $CsPbBr_3$ film. Reprinted with permission from ref. [39]. Copyright 2018 American Chemical

Society. Schematic diagram showing the two-step solution method via multi-step spin-coating and top-view SEM images of an inorganic $CsPbBr_3$ film. Reprinted with permission from ref. [40]. Copyright 2018 WILEY-VCH Verlag GmbH & Co. KGaA, Weinheim.

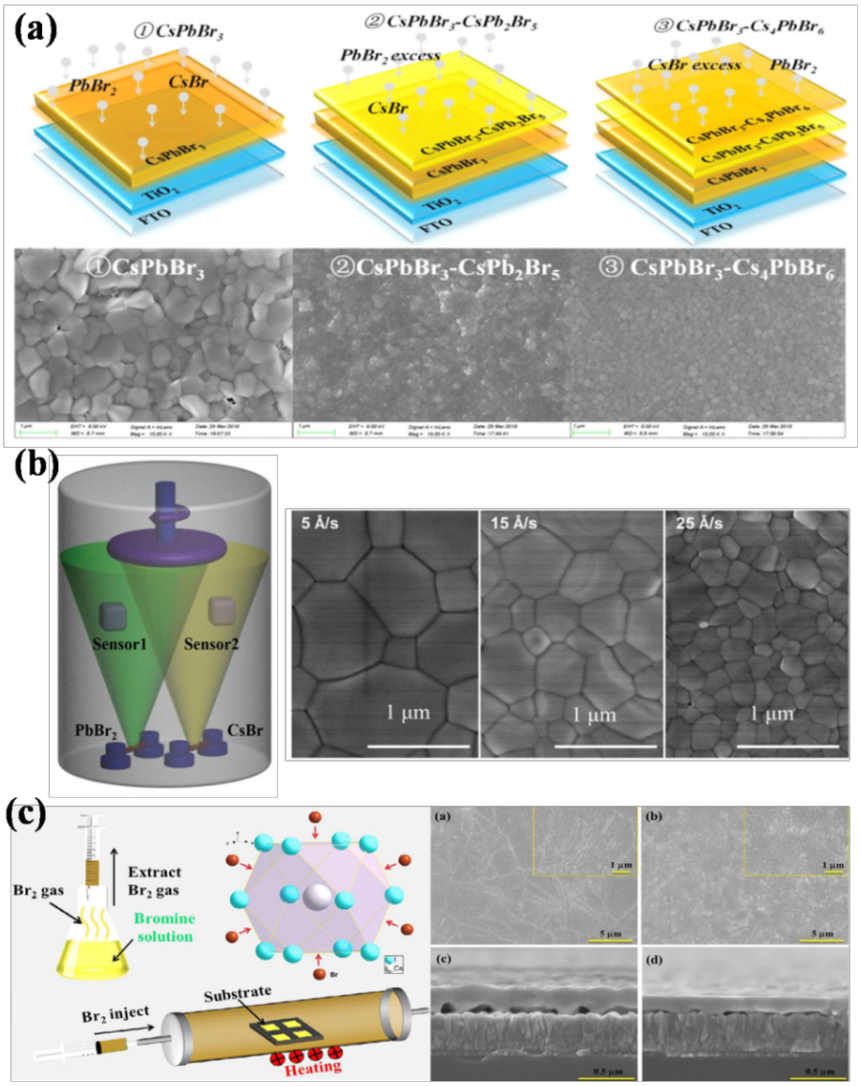


**Figure 3.** (a) Schematic diagram showing the sequential vapor deposition method for inorganic $CsPbBr_3$ solar cells and corresponding top-view SEM images of $CsPbBr_3$ films. Reprinted with permission from ref. [41]. Copyright 2019 WILEY-VCH Verlag GmbH & Co. KGaA, Weinheim. (b) Schematic diagram showing the co-evaporation method to deposit inorganic $CsPbBr_3$ thin films in vacuum and corresponding top-view SEM images of $CsPbBr_3$ films. Reprinted with permission from ref. [61]. Copyright 2018 WILEY-VCH Verlag GmbH & Co. KGaA, Weinheim. (c) Schematic diagram showing the vapor-assisted CVD process to produce $CsPbBr_3$ films and corresponding

top-view and cross-section SEM images of $CsPbBr_3$ films. Reprinted with permission from ref. [62]. Copyright 2018 Elsevier Ltd.

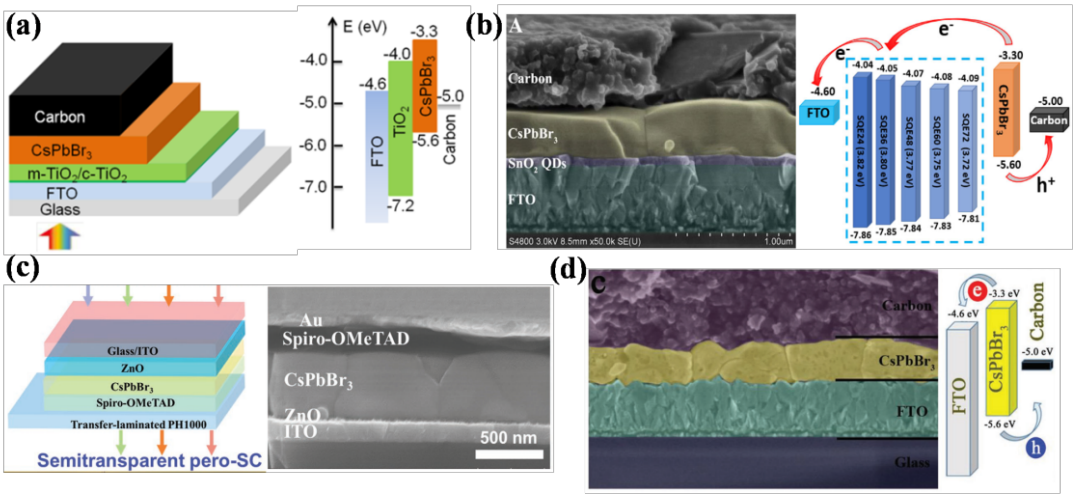


**Figure 4.** Schematic illustration of $CsPbBr_3$ solar cells with different electron transport layers (ETLs): (a) $TiO_2$ ETL, reprinted with permission from ref. [31]. Copyright 2016 American Chemical Society. (b) $SnO_2$ ETL, reprinted with permission from ref. [69]. Copyright 2018 WILEY-VCH Verlag GmbH & Co. KGaA, Weinheim. (c) ZnO, reprinted with permission from ref. [61]. Copyright 2018 WILEY-VCH Verlag GmbH & Co. KGaA, Weinheim. (d) Without ETL, reprinted with permission from ref. [79]. Copyright 2018 WILEY-VCH Verlag GmbH & Co. KGaA, Weinheim.

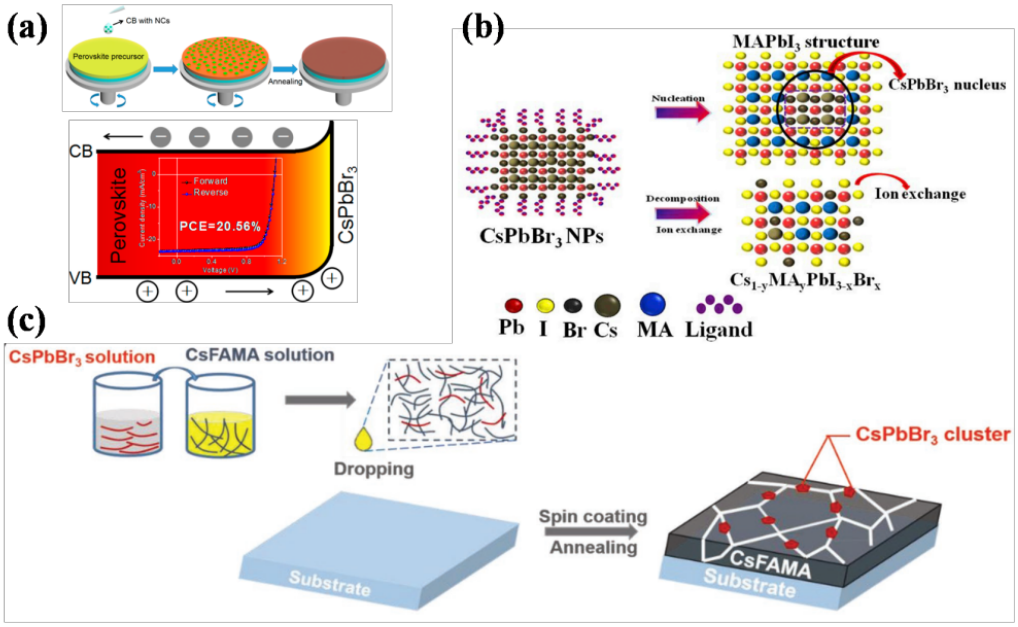


**Figure 5.** Schematic illustration of (a) $CsPbBr_3$ NCs, reprinted with permission from ref. [71]. Copyright 2017 American Chemical Society. (b) $CsPbBr_3$ NPs, reprinted with permission from ref. [73]. Copyright 2019 Elsevier Ltd. (c) $CsPbBr_3$ cluster as an interlayer in hybrid PSCs. Reprinted with permission from ref. [72]. Copyright 2018 WILEY-VCH Verlag GmbH & Co. KGaA, Weinheim.

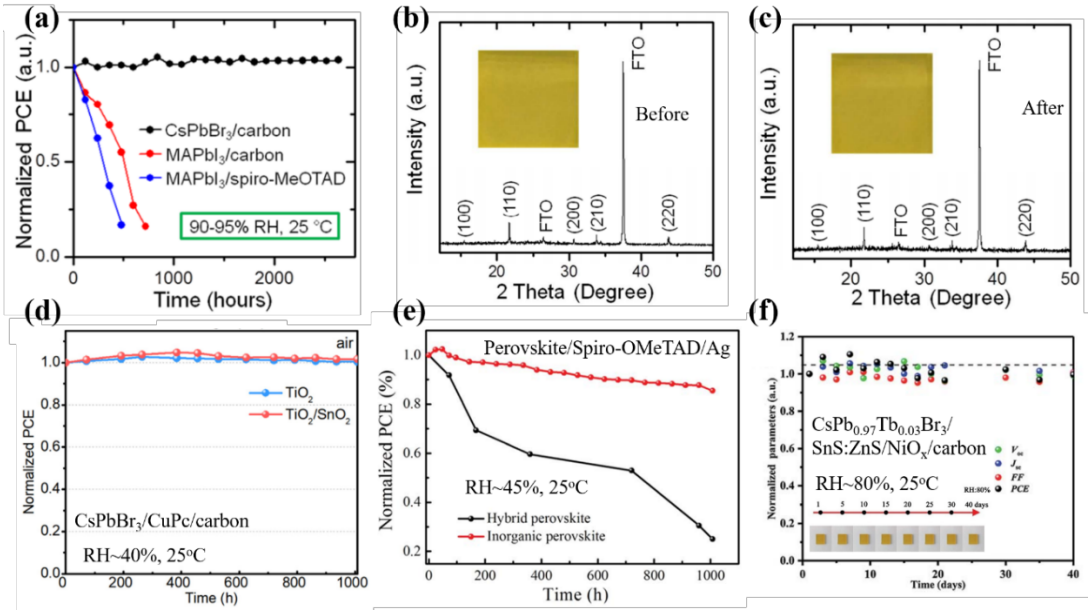


**Figure 6.** (a) Long-term stability of $CsPbBr_3$/carbon PSC as a function of storage time in humid air (90-95% RH, 25 °C). As comparison, $MAPbI_3$/carbon and $MAPbI_3$/spiro-OMeTAD show fast degradation profiles. (b, c) XRD characterization of pristine $CsPbBr_3$ film (b) before and (c) after stored in high moisture condition (90-95% RH, 25 °C) for 15 days. Reprinted with permission from ref. [31]. Copyright 2016 American Chemical Society. (d) Durability of the $TiO_2$- and $TiO_2/SnO_2$-based ETL $CsPbBr_3$ PSCs ($CsPbBr_3$/CuPC/carbon) when stored in ambient air with ~ 40% RH at room temperature (25 °C) for over 1000 h. Reprinted with permission from ref. [53]. Copyright 2019 Elsevier Ltd. (e) Stability tests of the hybrid and inorganic PSCs (Perovskite/Spiro-OMeTAD/Ag) under a humidity of ~45%. Reprinted with permission from ref. [60]. Copyright 2018 Royal Society of Chemistry. (f) Normalized $V_{oc}$, $J_{sc}$, FF, and PCE of FTO/c-$TiO_2$/m-$TiO_2$/$CsPb_{0.97}Tb_{0.03}Br_3$/SnS:ZnS/NiOx/carbon PSC without encapsulation. Reprinted with permission from ref. [105]. Copyright 2018 Royal Society of Chemistry.

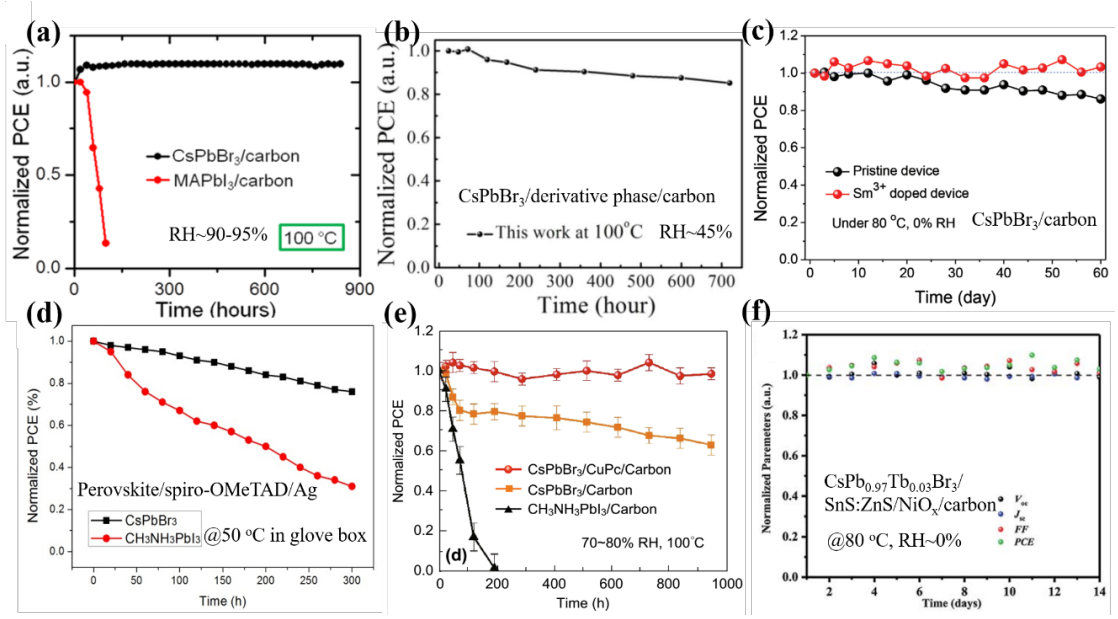


**Figure 7.** (a) Normalized PCEs of the FTO/$TiO_2$/$CsPbBr_3$/carbon-based PSCs and $MAPbI_3$/carbon-based hybrid PSCs at high temperature (100 °C) treatment without encapsulation. Reprinted with permission from ref. [31]. 2016 American Chemical Society. (b) Thermal stability of $CsPbBr_3$ carbon-based PSCs incorporated with the derivative phase (FTO/$TiO_2$/$CsPbBr_3$/$CsPbBr_3$-$CsPb_2Br_5$/$CsPbBr_3$-$Cs_4PbBr_6$/carbon) at 100 °C for over 700 h. Reprinted with permission from ref. [41]. Copyright 2019 WILEY-VCH Verlag GmbH & Co. KGaA, Weinheim. (c) Long-term stability of $CsPbBr_3$ carbon-based PSCs (FTO/$TiO_2$/$CsPbBr_3$/carbon) with / without $Sm^{3+}$ doping at 80 °C and 0% RH for 60 days. Reprinted with permission from ref. [68]. Copyright 2018 WILEY-VCH Verlag GmbH & Co. KGaA, Weinheim. (d) Durability of the spiro-OMeTAD HTL-based $CsPbBr_3$ PSCs (FTO/$TiO_2$/perovskite/spiro-OMeTAD/Ag) when stored at 50 °C for over 300 h. Reprinted with permission from ref. [91]. Copyright 2017 Elsevier Ltd. (e) Durability of the CuPc HTL-based $CsPbBr_3$ PSCs (FTO/$TiO_2$/$CsPbBr_3$/CuPc/carbon) when stored at 100 °C for 1000 h. As comparison,

the PSCs based on $MAPbI_3$/carbon and $CsPbBr_3$/carbon showed fast degradation profiles. Reprinted with permission from ref. [84]. Copyright 2018 Springer International Publishing. (f) Normalized $V_{oc}$, $J_{sc}$, FF, and PCE of the FTO/c-$TiO_2$/m-$TiO_2$/$CsPb_{0.97}Tb_{0.03}Br_3$/SnS:ZnS/$NiO_x$/carbon PSCs without encapsulation at 80 °C. Reprinted with permission from ref. [105]. Copyright 2018 Royal Society of Chemistry.

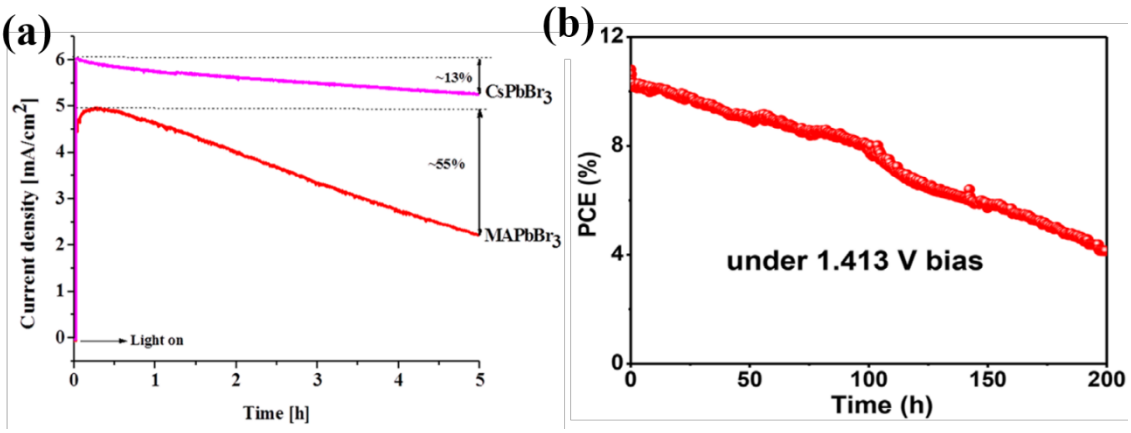


**Figure 8.** (a) Steady-state power outputs at the maximum power point of the $CsPbBr_3$ PSC with HTL. Reprinted with permission from ref. [96]. Copyright 2016 American Chemical Society. (b) Steady-state power outputs at the maximum power point of the $CsPbBr_3$ PSC with carbon electrode. Reprinted with permission from ref. [69]. Copyright 2019 WILEY-VCH Verlag GmbH & Co. KGaA, Weinheim.

**Table 1.** Summary of $CsPbBr_3$ PSCs in the literature.

| Device | Method | PCE [%] | $V_{oc}$ [V] | $J_{sc}$ [mA $cm^{-2}$] | FF [%] | Lifetime (Moisture/Heat) | | Ref |
|---|---|---|---|---|---|---|---|---|
| ITO/PEDOT:PSS/$CsPbBr_3$ /PCBM/Ag | Co-vapor | 3.9 | 0.94 | 5.9 | 70 | / | / | [85] |
| FTO/$TiO_2$/$CsPbBr_3$ QD/Spiro-OMeTAD/Au | 2-Solution | 4.21 | 0.859 | 8.55 | 57 | / | / | [94] |
| FTO/$TiO_2$/$CsPbBr_3$/CZTS/ Spiro-OMeTAD/Ag | 2-Solution | 5.36 | 1.12 | 7.04 | 68.11 | 2500 h Air | / | [70] |
| FTO/$TiO_2$/$CsPbBr_3$/PTAA/ Au | 2-Solution | 5.95 | 1.28 | 6.24 | 74 | / | / | [52] |
| FTO/$TiO_2$/$CsPbBr_3$/Spiro-OMeTAD/Au | 2-Solution | 6.05 | 1.34 | 6.52 | 69 | / | / | [95] |
| FTO/$TiO_2$/$CsPbBr_3$/PTAA/ Au | 2-Solution | 6.2 | 1.25 | 6.7 | 73 | 14 days RH~20% | / | [96] |
| FTO/$TiO_2$/$CsPbBr_3$(Cl)/Spiro-OMeTAD/Ag | 2-Solution | 6.21 | 1.02 | 8.47 | 71.6 | 300 h RH~40% | 300 h T~50°C | [91] |
| FTO/ZnO/$CsPbBr_3$-QDs/Spiro-OMeTAD/Au | 2-Solution | 6.81 | 1.43 | 6.17 | 77.2 | 100 days RH~45% | / | [82] |
| FTO/$TiO_2$/$CsPbBr_3$/Spiro-OMeTAD/Au | Co-vapor | 6.95 | 1.27 | 6.97 | 78.5 | 60 days RH~20% | / | [63] |
| FTO/ZnO/$CsPbBr_3$/Spiro-OMeTAD/Au | Co-vapor | 7.78 | 1.44 | 7.01 | 77.11 | / | / | [61] |
| FTO/$TiO_2$/$CsPbBr_3$/Si QDs/Spiro-OMeTAD/Ag | 1-Solution | 8.31 | 1.42 | 7.8 | 75 | 7 days RH~70% | / | [97] |
| FTO/$TiO_2$/$CsPbBr_3$/Spiro-OMeTAD/Ag | Sequential-vapor | 8.34 | 1.296 | 8.48 | 75.9 | 1000 h RH~45% | / | [60] |
| ITO/$SnO_2$/$CsPbBr_3$/Spiro-OMeTAD/Au | 1-Solution | 9.81 | 1.26 | 10.33 | 75.34 | / | / | [51] |
| FTO/$TiO_2$/PTI-$CsPbBr_3$ /Spiro-OMeTAD/Ag | Sequential-vapor | 10.91 | 1.498 | 9.78 | 74.47 | 1000 h RH~45% | 20 h T~100°C | [64] |
| FTO/$CsPbBr_3$/carbon | 2-Solution | 2.35 | 1.05 | 4.64 | 48.2 | / | / | [79] |
| FTO/$TiO_2$/$CsPbBr_3$/carbon | Solution&Vapor | 5.38 | 1.13 | 6.79 | 70.0 | 21 days Air | / | [63] |
| FTO/$TiO_2$/$CsPbBr_3$/carbon | 2-Solution | 5.86 | 1.34 | 6.46 | 68.04 | 240 h RH~60% | / | [39] |
| FTO/$TiO_2$/$CsPbBr_3$/carbon | 2-Solution | 6.1 | 1.38 | 7.13 | 62 | 200 days RH~25–85% | 1080 h T~80°C | [98] |
| FTO/$TiO_2$/$CsPbBr_3$/CuPC/ carbon | 2-Solution | 6.21 | 1.26 | 6.62 | 74.4 | 2000 h RH~40% | 944 h RH~80%, T~100°C | [84] |

| | | | | | | | | |
|---|---|---|---|---|---|---|---|---|
| FTO/$TiO_2$/$CsPbBr_3$/P3HT/carbon | 2-Solution | 6.49 | 1.36 | 7.02 | 68 | 40 days Air | / | [99] |
| FTO/$TiO_2$/$CsPbBr_3$/carbon | 2-Solution | 6.7 | 1.24 | 7.4 | 73 | 2640 h RH~90% | / | [31] |
| FTO/$TiO_2$/$CsPbBr_3$/carbon :PtNiNW | 2-Solution | 7.86 | 1.432 | 6.78 | 81.0 | 20 days RH~80% | / | [90] |
| FTO/$TiO_2$/m-$ZrO_2$/$CsPbBr_3$/carbon | 2-Solution | 8.19 | 1.44 | 7.75 | 73.52 | / | / | [100] |
| FTO/$TiO_2$/$CsPbBr_3$/carbon | 2-Solution | 8.63 | 1.37 | 7.66 | 82.22 | 90 days RH~10% | / | [101] |
| FTO/$TiO_2$/$SnO_2$/$CsPbBr_3$/CuPc/carbon | 2-Solution | 8.79 | 1.31 | 8.24 | 81.4 | 1000 h RH~40% | 30days T~60°C | [53] |
| FTO/$TiO_2$/$CsPbBr_3$/carbon | Co-vapor | 8.86 | 1.522 | 7.24 | 80.4 | / | 30 days RH~35%, T~85°C | [102] |
| FTO/$TiO_2$/$CsPbBr_3$/MXene/carbon | Sequential-vapor | 9.01 | 1.444 | 8.54 | 73.08 | 1900 h RH~45% | 600 h T~80°C | [103] |
| FTO/$TiO_2$/$CsPbBr_3$/carbon | 2-Solution | 9.72 | 1.458 | 8.12 | 82.1 | 130 days RH~90% | 40 days T~80°C | [40] |
| FTO/$TiO_2$/$CsPbBr_3$/P3HT/ZnPC/carbon | 2-Solution | 10.03 | 1.578 | 7.652 | 83.06 | 30 days RH~70% | / | [104] |
| FTO/$TiO_2$/$CsPb_{0.97}Sm_{0.03}Br_3$ /carbon | 2-Solution | 10.14 | 1.594 | 7.48 | 85.1 | 110 days RH~80% | 60 days T~80°C | [68] |
| FTO/$TiO_2$/$CsPbBr_3$/carbon | Sequential-vapor | 10.17 | 1.461 | 9.24 | 75.39 | 3000 h RH~45% | 700 h T~100°C | [41] |
| FTO/$TiO_2$/$CsPb_{0.97}Tb_{0.03}Br_3$/SnS:ZnS/$NiO_x$/carbon | 2-Solution | 10.26 | 1.57 | 8.21 | 79.6 | 40 days RH~80% | 14 days T~80°C | [105] |
| FTO/$TiO_2$/$CsPbBr_3$/MnS/carbon | Solution&Vapor | 10.45 | 1.52 | 8.28 | 83 | 150 days RH~80% | 100 days T~80°C | [106] |
| FTO/$SnO_2$ QDs/$CsPbBr_3$/$CsSnBr_3$ QD /carbon | 2-Solution | 10.6 | 1.61 | 7.8 | 84.4 | 10 days RH~80% | 10 days T~80°C | [69] |
| FTO/$TiO_2$/$CsPbBr_3$/Cu(Cr,M)$O_2$/carbon | 2-Solution | 10.79 | 1.615 | 7.81 | 85.5 | 60 days RH~80% | 40 days T~80°C | [107] |

(※1-Solution stands for the one-step solution method; 2-Solution stands for the two-step solution method.)

**TOC**

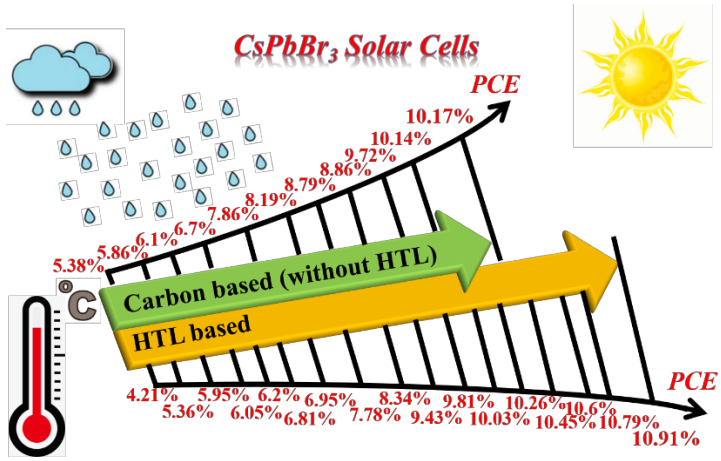


**Inorganic perovskite solar cells:** Recent progress of all bromide inorganic perovskite solar cells combined with processing techniques, devices structure, efficiency and stability are reviewed. Hole-transport layer based $CsPbBr_3$ solar cells show a rapid increasing efficiency and carbon electrode structure ensures a long-term stability in moisture and thermal condition.

**Biographies**

**Guoqing Tong** received his B.Sc. in 2011, M. S. in 2014 and Ph.D. in 2016 from Hefei University, Hefei University of Technology and Nanjing University, respectively. Then he joined Hefei University of Technology as a research assistant. Now he is a postdoctoral scholar in Prof. Yabing Qi's research unit (Energy Materials and Surface Sciences Unit) at Okinawa Institute of Science and Technology Graduate University (OIST). His research interests mainly focus on the vapor growth of perovskite materials and the application of perovskite in solar cells and photodetectors.

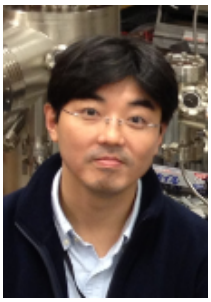

**Luis K. Ono** is a staff scientist in Prof. Yabing Qi's research unit (Energy Materials and Surface Sciences Unit) at Okinawa Institute of Science and Technology Graduate University in Japan. He obtained his B.S. in Physics/Microelectronics from the University of São Paulo, Brazil. Later he joined the Department of Nuclear Engineering in Kyoto University, Japan, and the University of Central Florida, USA, where he obtained his M.S. and Ph.D., respectively. His current research focuses are on the fundamental understanding and surface science aspects of perovskite solar cells (https://groups.oist.jp/emssu).

**Yabing Qi** is Professor and Unit Director of Energy Materials and Surface Sciences Unit at Okinawa Institute of Science and Technology Graduate University in Japan.

Prior to his current appointment, Prof. Qi was a postdoctoral fellow at Princeton University. He received his B.S., M.Phil., and Ph.D. from Nanjing University, Hong Kong University of Science and Technology, and University of California Berkeley, respectively. His research interests include perovskite solar cells, surface sciences, energy materials, and organic electronics. (https://groups.oist.jp/emssu)